Available online at www.sciencedirect.com

ScienceDirect

International Journal of Solids and Structures 44 (2007) 1461–1487

INTERNATIONAL JOURNAL OF SOLIDS and STRUCTURES

www.elsevier.com/locate/ijsolstr

Postbuckling of double-walled carbon nanotubes with temperature dependent properties and initial defects under combined axial and radial mechanical loads

Hui-Shen Shen *, Chen-Li Zhang

Department of Engineering Mechanics, Shanghai Jiao Tong University, Shanghai 200030, People's Republic of China

Received 22 February 2006; received in revised form 12 June 2006
Available online 23 June 2006

Abstract

Buckling and postbuckling analysis is presented for a double-walled carbon nanotube subjected to combined axial and radial loads in thermal environments. The analysis is based on a continuum mechanics model in which each tube of a double-walled carbon nanotube is described as an individual orthotropic shell with presence of van der Waals interaction forces and the interlayer friction is negligible between the inner and outer tubes. The governing equations are based on higher order shear deformation shell theory with a von Kármán-Donnell-type of kinematic nonlinearity and include thermal effects. Temperature-dependent material properties, which come from molecular dynamics simulations, and initial point defect, which is simulated as a dimple on the tube wall, are both taken into account. A singular perturbation technique is employed to determine the interactive buckling loads and postbuckling equilibrium paths. The numerical illustrations concern the postbuckling response of perfect and imperfect, double-walled carbon nanotubes subjected to combined axial and radial mechanical loads under different sets of thermal environments. The results reveal that temperature change only has a small effect on the postbuckling behavior of the double-walled carbon nanotube. The axially-loaded double-walled carbon nanotube subjected to radial pressure has an unstable postbuckling path, and the structure is imperfection–sensitive. In contrast, the pressure-loaded double-walled carbon nanotube subjected to axial compression has a very weak "snap-through" postbuckling path, and the structure is virtually imperfection–insensitive.

Keywords: Buckling; Postbuckling; Nanotube; Continuum shell model; Higher order shear deformable shell theory; Temperature-dependent properties; Initial point defects

1. Introduction

Recently, a new class of promising materials known as carbon nanotubes (CNTs) has drawn considerable attention. Determining their material properties, including physical, chemical, electrical and mechanical

* Corresponding author.
E-mail address: hsshen@mail.sjtu.edu.cn (H.-S. Shen).

0020-7683/$ - see front matter © 2006 Elsevier Ltd. All rights reserved.
doi:10.1016/j.ijsolstr.2006.06.027

properties, are the topics of investigations (Iijima, 1991; Treacy et al., 1996; Lu, 1997; Lourie and Wagner, 1998; Zhou et al., 2000; Ru, 2000b,c; Kudin et al., 2001; Tu and Ou-Yang, 2002; Jin and Yuan, 2003; Pantano et al., 2004; Chang et al., 2005a). Instabilities in nanotubes have also been of substantial interest and many nanotube experiments have observed buckling (Iijima et al., 1996; Falvo et al., 1997; Thomsen et al., 1999; Elliott et al., 2004; Waters et al., 2004, 2005). However, direct experiments are themselves still under development due to the very small size of carbon nanotubes, the numerical simulation and the theoretical approaches are widely used to investigate buckling behavior of carbon nanotubes. Yakobson et al. (1996) presented a number of molecular dynamics (MD) simulations for single-walled carbon nanotubes under axial compression, bending and torsion, but they did not simulate nanotubes under hydrostatic pressure. In their study a remarkable synergism between the shell theory predictions and the MD results was found. They concluded that the critical deformations at which these buckling events occur could be estimated by a continuum shell model.

It has been reported in the literature that continuum shell model which is familiar to engineers may be applicable for the analysis of CNTs. Ru (2000a,b, 2001a,b) proposed a continuum shell model to study infinitesimal buckling of double-walled carbon nanotubes subjected to axial compression in the presence of the intertube van der Waals forces, but his solutions were approximate due to the assumption of equally axial stress resultants of the outer and inner tubes. This work was then extended to the case of multi-walled carbon nanotubes subjected to radial pressure (Wang et al., 2003a), and combined loading of axial compression and internal/external pressure (Wang et al., 2003b). Similar works did by Wang et al. (2005b), Wang and Yang (2006), Yang and Wang (2006) for multi-walled carbon nanotubes under torsion and bending. In these studies, the classical shell theory, i.e. the theory based on the Kirchhoff–Love hypothesis, is used and therefore the transverse shear deformation is usually not accounted for. It is well known the thin shell theory is adequate for cylindrical shells when the radius-to-thickness ratio is greater than 20. It has been shown (Yakobson et al., 1996; Jin and Yuan, 2003), most carbon nanotubes have low values of radius-to-thickness ratio. As a result, the continuum mechanics model for multi-walled carbon nanotubes requires the use of shear deformation shell theory and involves an interlayer van der Waals interaction. Based on a higher order shear deformation shell theory, Shen (2004) gave a postbuckling analysis of double-walled carbon nanotubes under hydrostatic pressure, and found that the applicability of continuum shell theory depends strongly on the effective material properties of nanotubes. However, a large variation of Young's modulus E and Poisson's ratio v, as well as effective wall thickness h was obtained and reported in the open literature. For example, from MD simulation results Yakobson et al. (1996) gave $E = 5.5$ TPa and $h = 0.066$ nm with $v = 0.19$. By using *ab initio* method, Kudin et al. (2001) obtained $E = 3.895$ TPa and $h = 0.0894$ nm with $v = 0.149$. By using an effective continuum/finite element approach, Pantano et al. (2004) obtained $E = 4.84$ TPa and $h = 0.075$ nm with $v = 0.19$. The differences of these results are in part due to the different models adopted and in part due to the different chirality and different size of carbon nanotubes. On the other hand, Halicioglu (1998) gave $v = 0.18$, $E = 0.5$ TPa and the effective wall thickness $h = 0.68$ nm, which is more than 10 times of that of Yakobson et al. (1996), and might cause a big problem. In the most continuum shell models the thickness of an individual carbon nanotube is usually taken to be $h = 0.34$ nm together with$E = 1.06$ TPa (Wang et al., 2003a,b; Wang et al., 2005a,b; Wang and Yang, 2006), which leads the pre-energy of such a shell is found to be about 26 times as large as the pre-energy of single-walled carbon nanotubes calculated using atomistic models. It is also questionable to take both the tube thickness and the intertube distance as 0.34 nm for multi-walled carbon nanotubes. It is noted that the Young's modulus reduces from 4.7 to 1.05 TPa, when the layer number of multi-walled carbon nanotubes increases from 1 to 100, as reported in Tu and Ou-Yang (2002). In fact, the material properties of carbon nanotubes are anisotropic, and chirality- and size-dependent (Jin and Yuan, 2003; Elliott et al., 2004; Wang et al., 2005; Chang et al., 2005a), and, therefore, all effective elastic properties adopted need to be carefully determined.

Recently, Chang et al. (2005b,c) examined the effect of tube size and chirality on the buckling of single-walled and/or multi-walled carbon nanotubes by using a molecular mechanics model. He et al. (2005a,b) examined the effect of intertube van der Waals interactions on the buckling behavior of multi-walled carbon nanotubes. They concluded that the greatest contribution to the van der Waals interaction comes from the adjacent layers and the contribution from a remote layer may be neglected. Wang et al. (2005a) studied the effect of temperature changes on the buckling behavior of multi-walled carbon nanotubes under axial com-

pression. In their study the formulations were based on the classical thin shell theory and the material properties were assumed to be temperature-independent. It has been shown (Ni et al., 2002) that the postbuckling behavior of an empty single-walled carbon nanotube subjected to axial compression depends on temperature. However, such an important effect is not accounted for in any of recent investigations (Chang et al., 2005b,c; Wang et al., 2005a; He et al., 2005a,b; Kitipornchai et al., 2005; Sears and Batra, 2006).

As we all known the initial geometric imperfection has a significant effect on the buckling and postbuckling behavior of pressure loaded cylindrical shells subjected to axial compression. It has been reported (Zhou, 1994; Ding, 2005) that single-walled and multi-walled carbon nanotubes contain local point defects. As a result, we need to know weather the postbuckling behavior of a pressure loaded carbon nanotube subjected to axial compression is still sensitive to this defect.

The present work attempts to solve this difficult problem, that is, to provide analytical solution for the postbuckling of double-walled carbon nanotubes with temperature dependent material properties and initial point defects subjected to combined axial and radial loads in thermal environments. Material properties are assumed to be temperature dependent and are obtained from MD simulations. An elastic double shell model with van der Waals interaction forces is proposed and each tube is described as an individual orthotropic shell and the interlayer friction is negligible between the inner and outer tubes. The governing equations are based on higher order shear deformation shell theory (HSDST) with a von Kármán- Donnell-type of kinematic nonlinearity and include thermal effects. The boundary layer theory suggested by Shen and Chen (1988, 1990) is extended to the case of double-walled carbon nanotubes. A singular perturbation technique is employed to determine the interactive buckling loads and postbuckling equilibrium paths. The nonlinear prebuckling deformations of the shell and the initial local defects, which are simulated as a dimple on the tube wall, are both taken into account. The numerical illustrations show the full nonlinear postbuckling response of perfect and imperfect, double-walled carbon nanotubes subjected to combined axial and radial mechanical loads under different sets of environmental conditions.

2. Theoretical development

Consider a double-walled carbon nanotube modeled as a shell system which is subjected to two loads combined out of a uniform radial pressure q and axial load P in thermal environments. The outer and inner tubes are assumed to have the same thickness h and length L, and have mean radii R_I and R_{II}, respectively, as shown in Fig. 1(a). Each shell is referred to a coordinate system (X, Y, Z) in which X and Y are in the axial and circumferential directions of the shell and Z is in the direction of the inward normal to the middle surface. The origin of the coordinate system is located at the center of each shell on the middle plane. The corresponding displacements are designated by $\overline{U}$, $\overline{V}$ and $\overline{W}$. $\overline{\Psi}_x$ and $\overline{\Psi}_y$ are the rotations of normals to the middle surface with respect to the Y- and X-axes, respectively. The shell is assumed to be orthotropic and to be geometrically imperfect. Denoting the initial local defect by $\overline{W}^*(X, Y)$, let $\overline{W}(X, Y)$ be the transverse deflection of each tube, and $\overline{F}(X, Y)$ be the stress function for the stress resultants defined by $\overline{N}_x = \overline{F}_{,yy}$, $\overline{N}_y = \overline{F}_{,xx}$ and $\overline{N}_{xy} = -\overline{F}_{,xy}$, where a comma denotes partial differentiation with respect to the corresponding coordinates.

Van der Waals forces are a kind of weak interactions between atoms that are not directly bonded together in the same molecular. In the present work the van der Waals interaction energy is estimated by using the much applied inverse power model, namely, Lennard–Jones pair potential (Girifalco and Lad, 1956; Girifalco, 1991), which contains two parts of the short-range repulsive interaction and the long-range attractive interaction. It has been shown (Girifalco and Lad, 1956; Girifalco, 1991), the van der Waals interaction force is a nonlinear function of the distance between two interacting atoms. It should be noted that we are only interested in the infinitesimal buckling of a carbon nanotube. Hence, in the present analysis, it is assumed that the interaction forces between the inner and outer shells are linearly proportional to the buckling deflection and can be expressed as $p = p_0 + C[\overline{W}_{II}(X, Y) - \overline{W}_I(X, Y)]$, in which and what follows the subscript I and II refer to the outer and inner tubes, respectively. This assumption is reasonably well when the interlayer distance is less than 0.425 nm. As will be seen later in Section 4, this condition can be satisfied in numerical analysis. On the other hand, since the curvature effects on the elastic property of graphene sheets are small (Thomsen et al., 1999), the initial stress due to the curvature of a carbon nanotube is neglected. In the above equation p_0 is a constant representing the initial uniform van der Waals pressure between two prior to buckling. In particular,

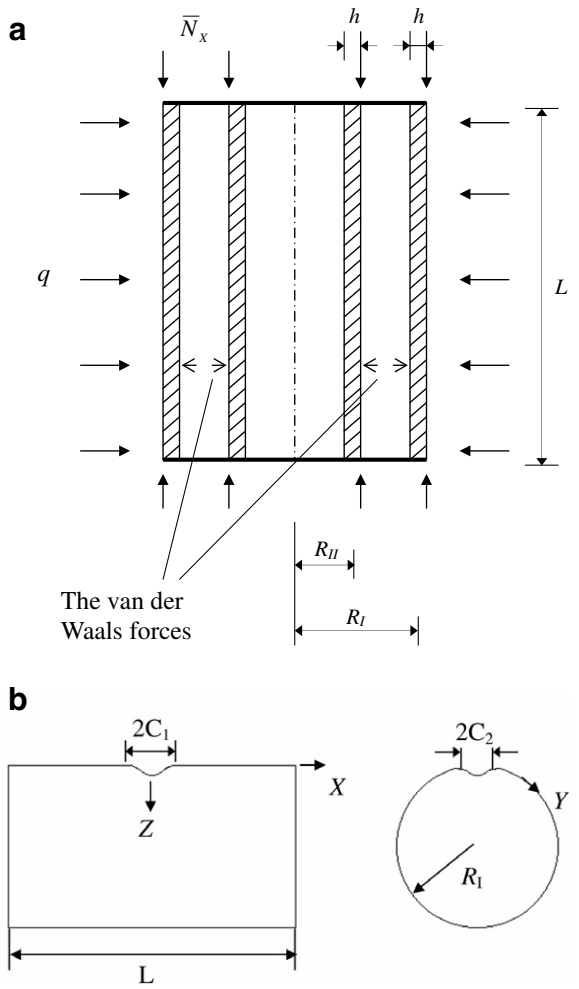

Fig. 1. An elastic shell model for a double-walled carbon nanotube under combined loading of axial compression and radial pressure: (a) geometry and loading case; (b) coordinate system and point defect.

the equilibrium distance between a carbon atom and a flat monolayer is around 0.34 nm (Girifalco, 1991), so that the initial pressure p_0 between the inner and outer tubes is zero or negligible if the initial interlayer spacing is 0.34 nm. C is a constant which was taken to be 61.9917 GPa/nm in Ru (2001b), and 99.1867 GPa/nm in Wang et al. (2003b). In fact, C can be estimated as the second derivative of the van der Waals energy-interlayer spacing. To account for the tube size effect and to include two parts of the repulsive and attractive interactions, from He et al. (2005a) we have

$$C = \frac{1001\pi\varepsilon_0\sigma_0^{12}R_{II}}{6d^4R_I^{13}}\int_0^{\pi}\frac{1}{[1-2\gamma_0\cos\theta+\gamma_0^2]^{13/2}}\,\mathrm{d}\theta - \frac{560\pi\varepsilon_0\sigma_0^{6}R_{II}}{9d^4R_I^{7}}\int_0^{\pi}\frac{1}{[1-2\gamma_0\cos\theta+\gamma_0^2]^{7/2}}\,\mathrm{d}\theta \tag{1}$$

where $\gamma_0 = R_{II}/R_I$, $d = 0.142$ nm is the C–C bond length, ε_0 is the depth of the potential, and σ_0 is a parameter that is determined by the equilibrium distance.

It has been shown (Cumings and Zettl, 2000; Kolmogorov and Crespi, 2000) the friction energy barrier between adjacent tubes is so low that the tubes could almost freely slid and rotate toward each other. We assume that no sliding occurs between the outer and inner tubes. We also assume that the tube is empty, and no initial internal pressure exists. Based on higher order shear deformation shell theory (Reddy and Liu, 1985), the Kármán-Donnell-type nonlinear differential equations for the outer tube, including van der Waals interaction forces and thermal effects, have readily been derived and can be expressed in terms of a

stress function $\overline{F}_I$, two rotations $\overline{\Psi}_{xI}$ and $\overline{\Psi}_{yI}$, and two transverse displacements $\overline{W}_I$ and $\overline{W}_{II}$, along with the initial geometric imperfection $\overline{W}_I^*$. They are

$$\widetilde{L}_{11}(\overline{W}_I) - \widetilde{L}_{12}(\overline{\Psi}_{xI}) - \widetilde{L}_{13}(\overline{\Psi}_{yI}) - \widetilde{L}_{16}(\overline{M}^T) - \frac{1}{R_I}\overline{F}_{I,xx} = \widetilde{L}(\overline{W}_I + \overline{W}_I^*, \overline{F}_I) + p_0 + C(\overline{W}_{II} - \overline{W}_I) + q \tag{2}$$

$$\widetilde{L}_{21}(\overline{F}_I) - \widetilde{L}_{25}(\overline{N}^T) + \frac{1}{R_I}\overline{W}_{I,xx} = -\frac{1}{2}\widetilde{L}(\overline{W}_I + 2\overline{W}_I^*, \overline{W}_I) \tag{3}$$

$$\widetilde{L}_{31}(\overline{W}_I) + \widetilde{L}_{32}(\overline{\Psi}_{xI}) - \widetilde{L}_{33}(\overline{\Psi}_{yI}) - \widetilde{L}_{36}(\overline{S}^T) = 0 \tag{4}$$

$$\widetilde{L}_{41}(\overline{W}_I) - \widetilde{L}_{42}(\overline{\Psi}_{xI}) + \widetilde{L}_{43}(\overline{\Psi}_{yI}) - \widetilde{L}_{46}(\overline{S}^T) = 0 \tag{5}$$

and for the inner tube they are

$$\widetilde{L}_{11}(\overline{W}_{II}) - \widetilde{L}_{12}(\overline{\Psi}_{xII}) - \widetilde{L}_{13}(\overline{\Psi}_{yII}) - \widetilde{L}_{16}(\overline{M}^T) - \frac{1}{R_{II}}\overline{F}_{II,xx} = \widetilde{L}(\overline{W}_{II} + \overline{W}_{II}^*, \overline{F}_{II}) - \frac{R_I}{R_{II}}[p_0 + C(\overline{W}_{II} - \overline{W}_I)] \tag{6}$$

$$\widetilde{L}_{21}(\overline{F}_{II}) - \widetilde{L}_{25}(\overline{N}^T) + \frac{1}{R_{II}}\overline{W}_{II,xx} = -\frac{1}{2}\widetilde{L}(\overline{W}_{II} + 2\overline{W}_{II}^*, \overline{W}_{II}) \tag{7}$$

$$\widetilde{L}_{31}(\overline{W}_{II}) + \widetilde{L}_{32}(\overline{\Psi}_{xII}) - \widetilde{L}_{33}(\overline{\Psi}_{yII}) - \widetilde{L}_{36}(\overline{S}^T) = 0 \tag{8}$$

$$\widetilde{L}_{41}(\overline{W}_{II}) - \widetilde{L}_{42}(\overline{\Psi}_{xII}) + \widetilde{L}_{43}(\overline{\Psi}_{yII}) - \widetilde{L}_{46}(\overline{S}^T) = 0 \tag{9}$$

where

$$\begin{aligned}
\widetilde{L}_{16}(\overline{M}^T) &= \frac{\partial^2}{\partial X^2}(\overline{M}_x^T) + 2\frac{\partial^2}{\partial X \partial Y}(\overline{M}_{xy}^T) + \frac{\partial^2}{\partial Y^2}(\overline{M}_y^T) \\
\widetilde{L}_{25}(\overline{N}^T) &= \left(A_{12}^*\frac{\partial^2}{\partial X^2} + A_{11}^*\frac{\partial^2}{\partial Y^2}\right)(\overline{N}_x^T) - A_{66}^*\frac{\partial^2}{\partial X \partial Y}(\overline{N}_{xy}^T) + \left(A_{22}^*\frac{\partial^2}{\partial X^2} + A_{12}^*\frac{\partial^2}{\partial Y^2}\right)(\overline{N}_y^T) \\
\widetilde{L}_{36}(\overline{S}^T) &= \frac{\partial}{\partial X}(\overline{S}_x^T) + \frac{\partial}{\partial Y}(\overline{S}_{xy}^T) \\
\widetilde{L}_{46}(\overline{S}^T) &= \frac{\partial}{\partial X}(\overline{S}_{xy}^T) + \frac{\partial}{\partial Y}(\overline{S}_y^T)
\end{aligned} \tag{10}$$

and all other linear operators $\widetilde{L}_{ij}()$ and nonlinear operator $\widetilde{L}()$ are defined as in Shen (2001). Since each tube is assumed to be orthotropic, the stretching/bending coupling is zero-valued, i.e. $B_{ij}^* = E_{ij}^* = 0$ in the present case. Note that Eqs. (2)–(9) are coupled and should be solved simultaneously.

It is assumed that the effective Young's moduli E_{11} and E_{22}, shear moduli G_{12}, G_{13} and G_{23}, and thermal expansion coefficients α_{11} and α_{22} of each tube are temperature-dependent, whereas Poisson's ratio v_{12} depends weakly on temperature change and is assumed to be a constant. The thermal forces $\overline{N}^T$, moments $\overline{M}^T$ and $\overline{S}^T$, and higher order moments $\overline{P}^T$ caused by elevated temperature are defined by

$$\begin{bmatrix} \overline{N}_x^T & \overline{M}_x^T & \overline{P}_x^T \\ \overline{N}_y^T & \overline{M}_y^T & \overline{P}_y^T \\ \overline{N}_{xy}^T & \overline{M}_{xy}^T & \overline{P}_{xy}^T \end{bmatrix} = \int_{-h/2}^{+h/2} \begin{bmatrix} A_x(T) \\ A_y(T) \\ A_{xy}(T) \end{bmatrix} (1, Z, Z^3)\Delta T \, \mathrm{d}Z \tag{11a}$$

and

$$\begin{bmatrix} \overline{S}_x^T \\ \overline{S}_y^T \\ \overline{S}_{xy}^T \end{bmatrix} = \begin{bmatrix} \overline{M}_x^T \\ \overline{M}_y^T \\ \overline{M}_{xy}^T \end{bmatrix} - \frac{4}{3h^2}\begin{bmatrix} \overline{P}_x^T \\ \overline{P}_y^T \\ \overline{P}_{xy}^T \end{bmatrix} \tag{11b}$$

where $\Delta T = T - T_0$ is temperature rise from some reference temperature T_0 at which there are no thermal strains, and

$$\begin{bmatrix} A_x(T) \\ A_y(T) \\ A_{xy}(T) \end{bmatrix} = -\begin{bmatrix} \overline{Q}_{11}(T) & \overline{Q}_{12}(T) & \overline{Q}_{16}(T) \\ \overline{Q}_{12}(T) & \overline{Q}_{22}(T) & \overline{Q}_{26}(T) \\ \overline{Q}_{16}(T) & \overline{Q}_{26}(T) & \overline{Q}_{66}(T) \end{bmatrix} \begin{bmatrix} 1 & 0 \\ 0 & 1 \\ 0 & 0 \end{bmatrix} \begin{bmatrix} \alpha_{11}(T) \\ \alpha_{22}(T) \end{bmatrix} \tag{12}$$

in which $\overline{Q}_{ij}(T) = Q_{ij}(T)$ and

$$\begin{aligned} &Q_{11}(T) = \frac{E_{11}(T)}{1 - v_{12}v_{21}}, \quad Q_{22}(T) = \frac{E_{22}(T)}{1 - v_{12}v_{21}}, \quad Q_{12}(T) = \frac{v_{21}E_{11}(T)}{1 - v_{12}v_{21}}, \\ &Q_{16} = Q_{26} = 0, \quad Q_{44}(T) = G_{23}(T), \quad Q_{55}(T) = G_{13}(T), \quad Q_{66}(T) = G_{12}(T) \end{aligned} \tag{13}$$

From Eqs. (11) and (12) the thermal force $\overline{N}^T_{xy}$, the thermal moments $\overline{M}^T$, and the higher order moments $\overline{P}^T$ are all zero valued, and $\overline{N}^T_x$ and $\overline{N}^T_y$ are both constants, so that $\widetilde{L}_{25}(\overline{N}^T) = \widetilde{L}_{16}(\overline{M}^T) = \widetilde{L}_{36}(\overline{S}^T) = \widetilde{L}_{46}(\overline{S}^T) = 0$.

The point defect is a basic and important geometric imperfection in carbon nanotubes, which may be modeled as a dimple in the outer tube or in both outer and inner tubes. We assume that the point defect located in the center of the carbon nanotubes can be expressed as

$$\overline{W}^*(X, Y) = A_m \exp\left(-\left|\frac{X}{C_1}\right| - \left|\frac{Y}{C_2}\right|\right) \tag{14}$$

where A_m is a small parameter characterizing the amplitude of the initial defect and C_1 and C_2 characterize the half-width of the region of the dimple, as shown in Fig 1(b).

The two end edges of both outer and inner tubes are assumed to be simply supported or clamped, so that the boundary conditions are $X = \pm L/2$:

$$\overline{W} = \overline{\Psi}_y = 0 \tag{15a}$$

$$\overline{M}_x = \overline{P}_x = 0 \quad \text{(simply supported)} \tag{15b}$$

$$\overline{\Psi}_x = 0 \quad \text{(clamped)} \tag{15c}$$

$$\int_0^{2\pi R_I} \overline{N}_{xI}\,\mathrm{d}Y + \int_0^{2\pi R_{II}} \overline{N}_{xII}\,\mathrm{d}Y + 2\pi(R_I + R_{II})h\sigma_x + \pi R_I^2 qa = 0 \tag{15d}$$

where $a = 0$ and $a = 1$ for lateral and hydrostatic pressure loading case, respectively, and σ_x is the average axial compressive stress, and $\overline{M}_x$ is the bending moment and $\overline{P}_x$ is higher order moment, as defined in Reddy and Liu (1985). Also we have the closed (or periodicity) condition for each tube

$$\int_0^{2\pi R_J} \frac{\partial \overline{V}}{\partial Y}\,\mathrm{d}Y = 0 \quad (J = I, II) \tag{16a}$$

or

$$\int_0^{2\pi R_J} \left[A^*_{22}\frac{\partial^2 \overline{F}}{\partial X^2} + A^*_{12}\frac{\partial^2 \overline{F}}{\partial Y^2} + \frac{\overline{W}}{R_J} - \frac{1}{2}\left(\frac{\partial \overline{W}}{\partial Y}\right)^2 - \frac{\partial \overline{W}}{\partial Y}\frac{\partial \overline{W}^*}{\partial Y} - (A^*_{12}\overline{N}^T_x + A^*_{22}\overline{N}^T_y)\right]\mathrm{d}Y = 0 \tag{16b}$$

Because of Eq. (16a), the in-plane boundary condition $\overline{V} = 0$ (at $X = \pm L/2$) is not needed in Eq. (15a).

It is assumed that the end-shortening displacements of the outer and inner tubes are identical. The average end-shortening relationship of each shell is defined as

$$\begin{aligned} \frac{\Delta_x}{L} &= -\frac{1}{2\pi R_J L}\int_0^{2\pi R_J}\int_{-L/2}^{+L/2} \frac{\partial \overline{U}}{\partial X}\,\mathrm{d}X\,\mathrm{d}Y \quad (J = I, II) \\ &= -\frac{1}{2\pi R_J L}\int_0^{2\pi R_J}\int_{-L/2}^{+L/2} \left[A^*_{11}\frac{\partial^2 \overline{F}}{\partial Y^2} + A^*_{12}\frac{\partial^2 \overline{F}}{\partial X^2} - \frac{1}{2}\left(\frac{\partial \overline{W}}{\partial X}\right)^2 - \frac{\partial \overline{W}}{\partial X}\frac{\partial \overline{W}^*}{\partial X} - (A^*_{11}\overline{N}^T_x + A^*_{12}\overline{N}^T_y)\right]\mathrm{d}X\,\mathrm{d}Y \end{aligned} \tag{17}$$

where Δ_x is shell end-shortening displacement in the X- direction.

In the above equations and what follows, the reduced stiffness matrices $[A^*_{ij}]$, $[D^*_{ij}]$, $[F^*_{ij}]$ and $[H^*_{ij}](i,j=1,2,6)$ are functions of temperature, determined through relationship (Shen, 2001)

$$\mathbf{A}^* = \mathbf{A}^{-1}, \quad \mathbf{D}^* = \mathbf{D}, \quad \mathbf{F}^* = \mathbf{F}, \quad \mathbf{H}^* = \mathbf{H} \tag{18a}$$

where A_{ij}, D_{ij} etc., are the shell stiffnesses, defined by

$$(A_{ij}, D_{ij}, F_{ij}, H_{ij}) = \int_{-h/2}^{+h/2} Q_{ij}(T)(1, Z^2, Z^4, Z^6)\,\mathrm{d}Z \quad (i,j=1,2,6) \tag{18b}$$

3. Solution methodology

Having developed the theory, we are in a position to solve Eqs. (2)–(9) with boundary conditions (15). Before proceeding, it is convenient first to define the following dimensionless quantities [with γ_{ijk} in Eqs. (29) and (A.11) below are defined as in Shen (2001)]

$$\begin{aligned}
&x = \pi\frac{X}{L}, \quad y = \frac{Y}{R_I}, \quad \beta = \frac{L}{\pi R_I}, \quad \varepsilon = \frac{\pi^2 R_I}{L^2}[D^*_{11}D^*_{22}A^*_{11}A^*_{22}]^{1/4}, \quad \gamma_0 = \frac{R_{II}}{R_I}, \quad C_0 = \frac{CL^4}{\pi^4[D^*_{11}D^*_{22}]^{1/2}}\\
&C_p = \frac{p_0 R_I}{\beta^2 D^*_{11}}[D^*_{11}D^*_{22}A^*_{11}A^*_{22}]^{1/2}, \quad \gamma_{14} = \left[\frac{D^*_{22}}{D^*_{11}}\right]^{1/2}, \quad \gamma_{24} = \left[\frac{A^*_{11}}{A^*_{22}}\right]^{1/2}, \quad \gamma_5 = -\frac{A^*_{12}}{A^*_{22}}\\
&(\gamma_{T1}, \gamma_{T2}) = (A^T_x, A^T_y)R_I\left[\frac{A^*_{11}A^*_{22}}{D^*_{11}D^*_{22}}\right]^{1/4}, \quad (\gamma_{C1}, \gamma_{C2}) = (L/\pi C_1, R_I/C_2)\\
&(W, W^*) = \varepsilon\frac{(\overline{W}, \overline{W}^*)}{[D^*_{11}D^*_{22}A^*_{11}A^*_{22}]^{1/4}}, \quad F = \varepsilon^2\frac{\overline{F}}{[D^*_{11}D^*_{22}]^{1/2}}, \quad (\Psi_x, \Psi_y) = \varepsilon^2\frac{L}{\pi}\frac{(\overline{\Psi}_x, \overline{\Psi}_y)}{[D^*_{11}D^*_{22}A^*_{11}A^*_{22}]^{1/4}}\\
&(M_x, P_x) = \varepsilon^2\frac{L^2}{\pi^2}\frac{1}{D^*_{11}[D^*_{11}D^*_{22}A^*_{11}A^*_{22}]^{1/4}}\left(\overline{M}_x, \frac{4}{3h^2}\overline{P}_x\right)\\
&\lambda_p = \frac{\sigma_x R_I h}{2}\left[\frac{A^*_{11}A^*_{22}}{D^*_{11}D^*_{22}}\right]^{1/4}, \quad \delta_p = \left(\frac{\Delta_x}{L}\right)\frac{R_I}{2[D^*_{11}D^*_{22}A^*_{11}A^*_{22}]^{1/4}}\\
&\lambda_q = q\frac{(3)^{3/4}LR_I^{3/2}[A^*_{11}A^*_{22}]^{1/8}}{4\pi[D^*_{11}D^*_{22}]^{3/8}}, \quad \delta_q = \left(\frac{\Delta_x}{L}\right)\frac{(3)^{3/4}LR_I^{1/2}}{4\pi[D^*_{11}D^*_{22}A^*_{11}A^*_{22}]^{3/8}}
\end{aligned} \tag{19}$$

in which $A^T_x = A^T_y$ are defined by

$$\begin{bmatrix} A^T_x \\ A^T_y \end{bmatrix} = -\int_{-h/2}^{h/2}\begin{bmatrix} A_x \\ A_y \end{bmatrix}\mathrm{d}Z \tag{20}$$

The nonlinear Eqs. (2)–(9) may then be written in dimensionless form as

$$\begin{aligned}
&\varepsilon^2[L_{11}(W_I) - C_0(W_{II} - W_I)] - \varepsilon L_{12}(\Psi_{xI}) - \varepsilon L_{13}(\Psi_{yI}) - \gamma_{14}F_{I,xx}\\
&\quad = \gamma_{14}\beta^2 L(W_I + W^*_I, F_I) + C_p + \gamma_{14}\frac{4}{3}(3)^{1/4}\lambda_q\varepsilon^{3/2}
\end{aligned} \tag{21}$$

$$L_{21}(F_I) + \gamma_{24}W_{I,xx} = -\frac{1}{2}\gamma_{24}\beta^2 L(W_I + 2W^*_I, W_I) \tag{22}$$

$$\varepsilon L_{31}(W_I) + L_{32}(\Psi_{xI}) - L_{33}(\Psi_{yI}) = 0 \tag{23}$$

$$\varepsilon L_{41}(W_I) - L_{42}(\Psi_{xI}) + L_{43}(\Psi_{yI}) = 0 \tag{24}$$

and

$$\begin{aligned}
&\varepsilon^2[\gamma_0 L_{11}(W_{II}) + C_0(W_{II} - W_I)] - \varepsilon\gamma_0 L_{12}(\Psi_{xII}) - \varepsilon\gamma_0 L_{13}(\Psi_{yII}) - \gamma_{14}F_{II,xx}\\
&\quad = \gamma_0\gamma_{14}\beta^2 L(W_{II} + W^*_{II}, F_{II}) - C_p
\end{aligned} \tag{25}$$

$$\gamma_0 L_{21}(F_{II}) + \gamma_{24} W_{II,xx} = -\frac{1}{2}\gamma_0\gamma_{24}\beta^2 L(W_{II} + 2W^*_{II}, W_{II}) \tag{26}$$

$$\varepsilon L_{31}(W_{II}) + L_{32}(\Psi_{xII}) - L_{33}(\Psi_{yII}) = 0 \tag{27}$$

$$\varepsilon L_{41}(W_{II}) - L_{42}(\Psi_{xII}) + L_{43}(\Psi_{yII}) = 0 \tag{28}$$

where

$$\begin{aligned}
L_{11}() &= \gamma_{110}\frac{\partial^4}{\partial x^4} + 2\gamma_{112}\beta^2\frac{\partial^4}{\partial x^2\partial y^2} + \gamma_{114}\beta^4\frac{\partial^4}{\partial y^4}\\
L_{12}() &= \gamma_{120}\frac{\partial^3}{\partial x^3} + \gamma_{122}\beta^2\frac{\partial^3}{\partial x\partial y^2}\\
L_{13}() &= \gamma_{131}\beta\frac{\partial^3}{\partial x^2\partial y} + \gamma_{133}\beta^3\frac{\partial^3}{\partial y^3}\\
L_{21}() &= \frac{\partial^4}{\partial x^4} + 2\beta^2\frac{\partial^4}{\partial x^2\partial y^2} + \beta^4\frac{\partial^4}{\partial y^4}\\
L_{31}() &= \gamma_{31}\frac{\partial}{\partial x} + \gamma_{310}\frac{\partial^3}{\partial x^3} + \gamma_{312}\beta^2\frac{\partial^3}{\partial x\partial y^2}\\
L_{32}() &= \gamma_{31} - \gamma_{320}\frac{\partial^2}{\partial x^2} - \gamma_{322}\beta^2\frac{\partial^2}{\partial y^2}\\
L_{33}() &= \gamma_{331}\beta\frac{\partial^2}{\partial x\partial y}\\
L_{41}() &= \gamma_{41}\beta\frac{\partial}{\partial y} + \gamma_{411}\beta\frac{\partial^3}{\partial x^2\partial y} + \gamma_{413}\beta^3\frac{\partial^3}{\partial y^3}\\
L_{42}() &= L_{33}()\\
L_{43}() &= \gamma_{41} - \gamma_{430}\frac{\partial^2}{\partial x^2} - \gamma_{432}\beta^2\frac{\partial^2}{\partial y^2}\\
L() &= \frac{\partial^2}{\partial x^2}\frac{\partial^2}{\partial y^2} - 2\frac{\partial^2}{\partial x\partial y}\frac{\partial^2}{\partial x\partial y} + \frac{\partial^2}{\partial y^2}\frac{\partial^2}{\partial x^2}
\end{aligned} \tag{29}$$

The boundary conditions of Eq. (15) become $x = \pm\pi/2$:

$$W = \Psi_y = 0 \tag{30a}$$

$$M_x = P_x = 0 \quad \text{(simply supported)} \tag{30b}$$

$$\Psi_x = 0 \quad \text{(clamped)} \tag{30c}$$

$$\frac{1}{2\pi}\int_0^{2\pi}\beta^2\frac{\partial^2 F_I}{\partial y^2}\,\mathrm{d}y + \frac{1}{2\pi}\int_0^{2\pi\gamma_0}\beta^2\frac{\partial^2 F_{II}}{\partial y^2}\,\mathrm{d}y + 2\lambda_p\varepsilon(1+\gamma_0) + \frac{2}{3}(3)^{1/4}\lambda_q\varepsilon^{3/2}a = 0 \tag{30d}$$

and the closed condition of Eq. (16b) becomes

$$\int_0^{2\pi}\left[\left(\frac{\partial^2 F_I}{\partial x^2} - \gamma_5\beta^2\frac{\partial^2 F_I}{\partial y^2}\right) + \gamma_{24}W_I - \frac{1}{2}\gamma_{24}\beta^2\left(\frac{\partial W_I}{\partial y}\right)^2 - \gamma_{24}\beta^2\frac{\partial W_I}{\partial y}\frac{\partial W^*_I}{\partial y} + \varepsilon(\gamma_{T2} - \gamma_5\gamma_{T1})\Delta T\right]\mathrm{d}y = 0 \tag{31}$$

In this section two loading conditions will be considered, so that the unit end-shortening relationship may be written in two dimensionless forms as

$$\begin{aligned}
\delta_q = -\frac{(3)^{3/4}}{8\pi^2\gamma_{24}}\varepsilon^{-3/2}\int_0^{2\pi}\int_{-\pi/2}^{+\pi/2}\Bigg[&\left(\gamma_{24}^2\beta^2\frac{\partial^2 F_I}{\partial y^2} - \gamma_5\frac{\partial^2 F_I}{\partial x^2}\right) - \frac{1}{2}\gamma_{24}\left(\frac{\partial W_I}{\partial x}\right)^2 - \gamma_{24}\frac{\partial W_I}{\partial x}\frac{\partial W^*_I}{\partial x}\\
&+\varepsilon(\gamma_{24}^2\gamma_{T1} - \gamma_5\gamma_{T2})\Delta T\Bigg]\mathrm{d}x\,\mathrm{d}y
\end{aligned} \tag{32a}$$

$$= -\frac{(3)^{3/4}}{8\pi^2\gamma_0\gamma_{24}}\varepsilon^{-3/2}\int_0^{2\pi\gamma_0}\int_{-\pi/2}^{+\pi/2}\left[\left(\gamma_{24}^2\beta^2\frac{\partial^2 F_{II}}{\partial y^2}-\gamma_5\frac{\partial^2 F_{II}}{\partial x^2}\right)-\frac{1}{2}\gamma_{24}\left(\frac{\partial W_{II}}{\partial x}\right)^2-\gamma_{24}\frac{\partial W_{II}}{\partial x}\frac{\partial W_{II}^*}{\partial x}\right.$$
$$\left.+\varepsilon(\gamma_{24}^2\gamma_{T1}-\gamma_5\gamma_{T2})\Delta T\right]\mathrm{d}x\,\mathrm{d}y \tag{32b}$$

and

$$\delta_p = -\frac{1}{4\pi^2\gamma_{24}}\varepsilon^{-1}\int_0^{2\pi}\int_{-\pi/2}^{+\pi/2}\left[\left(\gamma_{24}^2\beta^2\frac{\partial^2 F_I}{\partial y^2}-\gamma_5\frac{\partial^2 F_I}{\partial x^2}\right)-\frac{1}{2}\gamma_{24}\left(\frac{\partial W_I}{\partial x}\right)^2-\gamma_{24}\frac{\partial W_I}{\partial x}\frac{\partial W_I^*}{\partial x}\right.$$
$$\left.+\varepsilon(\gamma_{24}^2\gamma_{T1}-\gamma_5\gamma_{T2})\Delta T\right]\mathrm{d}x\,\mathrm{d}y \tag{32c}$$
$$= -\frac{1}{4\pi^2\gamma_0\gamma_{24}}\varepsilon^{-1}\int_0^{2\pi\gamma_0}\int_{-\pi/2}^{+\pi/2}\left[\left(\gamma_{24}^2\beta^2\frac{\partial^2 F_{II}}{\partial y^2}-\gamma_5\frac{\partial^2 F_{II}}{\partial x^2}\right)-\frac{1}{2}\gamma_{24}\left(\frac{\partial W_{II}}{\partial x}\right)^2-\gamma_{24}\frac{\partial W_{II}}{\partial x}\frac{\partial W_{II}^*}{\partial x}\right.$$
$$\left.+\varepsilon(\gamma_{24}^2\gamma_{T1}-\gamma_5\gamma_{T2})\Delta T\right]\mathrm{d}x\,\mathrm{d}y \tag{32d}$$

In Eq. (19), we introduce an important parameter ε. For most carbon nanotubes $[D_{11}^* D_{22}^* A_{11}^* A_{22}^*]^{1/4} \cong 0.3h$, hence when $\overline{Z} = (L^2/Rh) > 2.96$, we have $\varepsilon < 1$. In particular, if the single-walled carbon nanotube is assumed to be an isotropic shell, we have $\varepsilon = \pi^2/\overline{Z}_B\sqrt{12}$, where $\overline{Z}_B = (L^2/Rh)[1-\nu^2]^{1/2}$ is the Batdorf shell parameter, which should be greater than 2.85 in the case of classical linear buckling analysis (Batdorf, 1947). It has been shown (Jin and Yuan, 2003; Yakobson et al., 1996), carbon nanotubes will have large values of $\overline{Z}$, so that we always have $\varepsilon \ll 1$. When $\varepsilon < 1$, Eqs. (21)–(28) are of the boundary layer type and may then be solved by means of a singular perturbation technique. The essence of this procedure, in the present case, is to assume that

$$\begin{aligned}
W &= w(x,y,\varepsilon) + \widetilde{W}(x,\xi,y,\varepsilon) + \widehat{W}(x,\zeta,y,\varepsilon)\\
F &= f(x,y,\varepsilon) + \widetilde{F}(x,\xi,y,\varepsilon) + \widehat{F}(x,\zeta,y,\varepsilon)\\
\Psi_x &= \Psi_x(x,y,\varepsilon) + \widetilde{\Psi}_x(x,\xi,y,\varepsilon) + \widehat{\Psi}_x(x,\zeta,y,\varepsilon)\\
\Psi_y &= \Psi_y(x,y,\varepsilon) + \widetilde{\Psi}_y(x,\xi,y,\varepsilon) + \widehat{\Psi}_y(x,\zeta,y,\varepsilon)
\end{aligned} \tag{33}$$

where ε is a small perturbation parameter (provided $\overline{Z} > 2.96$) as defined in Eq. (19) and $w(x,y,\varepsilon)$, $f(x,y,\varepsilon)$, $\Psi_x(x,y,\varepsilon)$, $\Psi_y(x,y,\varepsilon)$ are called regular solutions of the shell, $\widetilde{W}(x,\xi,y,\varepsilon)$, $\widetilde{F}(x,\xi,y,\varepsilon)$, $\widetilde{\Psi}_x(x,\xi,y,\varepsilon)$, $\widetilde{\Psi}_y(x,\xi,y,\varepsilon)$ and $\widehat{W}(x,\zeta,y,\varepsilon)$, $\widehat{F}(x,\zeta,y,\varepsilon)$, $\widehat{\Psi}_x(x,\zeta,y,\varepsilon)$, $\widehat{\Psi}_y(x,\zeta,y,\varepsilon)$ are the boundary layer solutions near the $x = \pm\pi/2$ edges, respectively, and ξ and ζ are the boundary layer variables, defined as

$$\xi = (\pi/2 + x)/\sqrt{\varepsilon}, \quad \zeta = (\pi/2 - x)/\sqrt{\varepsilon} \tag{34}$$

This means for isotropic cylindrical shells the width of the boundary layers is of order $\sqrt{Rh}$. In Eq. (33) the regular and boundary layer solutions are taken in the forms of perturbation expansions as

$$w(x,y,\varepsilon) = \sum_{j=1}\varepsilon^{j/2}w_{j/2}(x,y), \quad f(x,y,\varepsilon) = \sum_{j=0}\varepsilon^{j/2}f_{j/2}(x,y)$$
$$\Psi_x(x,y,\varepsilon) = \sum_{j=1}\varepsilon^{j/2}(\Psi_x)_{j/2}(x,y), \quad \Psi_y(x,y,\varepsilon) = \sum_{j=1}\varepsilon^{j/2}(\Psi_y)_{j/2}(x,y) \tag{35a}$$
$$\widetilde{W}(x,\xi,y,\varepsilon) = \sum_{j=0}\varepsilon^{j/2+1}\widetilde{W}_{j/2+1}(x,\xi,y), \quad \widetilde{F}(x,\xi,y,\varepsilon) = \sum_{j=0}\varepsilon^{j/2+2}\widetilde{F}_{j/2+2}(x,\xi,y)$$
$$\widetilde{\Psi}_x(x,\xi,y,\varepsilon) = \sum_{j=0}\varepsilon^{(j+3)/2}(\widetilde{\Psi}_x)_{(j+3)/2}(x,\xi,y), \quad \widetilde{\Psi}_y(x,\xi,y,\varepsilon) = \sum_{j=0}\varepsilon^{j/2+2}(\widetilde{\Psi}_y)_{j/2+2}(x,\xi,y) \tag{35b}$$
$$\widehat{W}(x,\zeta,y,\varepsilon) = \sum_{j=0}\varepsilon^{j/2+1}\widehat{W}_{j/2+1}(x,\zeta,y), \quad \widehat{F}(x,\zeta,y,\varepsilon) = \sum_{j=0}\varepsilon^{j/2+2}\widehat{F}_{j/2+2}(x,\zeta,y)$$
$$\widehat{\Psi}_x(x,\zeta,y,\varepsilon) = \sum_{j=0}\varepsilon^{(j+3)/2}(\widehat{\Psi}_x)_{(j+3)/2}(x,\zeta,y), \quad \widehat{\Psi}_y(x,\zeta,y,\varepsilon) = \sum_{j=0}\varepsilon^{j/2+2}(\widehat{\Psi}_y)_{j/2+2}(x,\zeta,y) \tag{35c}$$

The initial buckling mode is assumed to have the form

$$w_I^{(2)}(x,y) = A_{11}^{(2)} \cos mx \cos ny \tag{36a}$$

$$w_{II}^{(2)}(x,y) = \chi_1 A_{11}^{(2)} \cos mx \cos ny \tag{36b}$$

in which χ_1 is a constant and can be determined later.

The initial point defects are assumed to be in both outer and inner tubes, i.e. $W_I^* = W_{II}^* = W^*$. This initial local geometric imperfection is represented as a Fourier cosine series as

$$W^*(x,y,\varepsilon) = \varepsilon^2 a_m \exp(-\gamma_{C1}|x| - \gamma_{C2}|y|) = \varepsilon^2 \mu A_{11}^{(2)} \left(\frac{a_0}{2} + \sum_{i=1} a_i \cos ix\right)\left(\frac{b_0}{2} + \sum_{j=1} b_j \cos jy\right) \tag{37a}$$

where

$$a_I = \frac{4}{\pi}\int_0^{\pi/2} \exp(-\gamma_{C1}x)\cos ix\,\mathrm{d}x, \quad b_j = \frac{2}{\pi}\int_0^{\pi} \exp(-\gamma_{C2}y)\cos jy\,\mathrm{d}y \tag{37b}$$

and $\mu = a_m/A_{11}^{(2)}$ is the imperfection parameter.

Substituting Eqs. (33)–(35) into Eqs. (21)–(28), and collecting terms of the same order of ε, we obtain three sets of perturbation equations for the regular and boundary layer solutions, respectively, the details of which may be found in Shen (2002). It has been shown (Shen and Chen, 1988, 1990) that the effect of the boundary layer on the buckling load of the shell under axial compression is quite different from that of the shell subjected to external pressure. To this end, two kinds of loading conditions will be considered.

Case (1) high values of external pressure combined with relatively low axial load. Let

$$\frac{P}{\pi R_I^2 q} = d_1 \tag{38a}$$

or

$$\frac{2\lambda_p \varepsilon}{\frac{4}{3}(3)^{1/4}\lambda_q \varepsilon^{3/2}} = \frac{d_1}{2} \tag{38b}$$

In this case, the boundary condition of Eq. (30d) becomes

$$\frac{1}{2\pi}\int_0^{2\pi} \beta^2 \frac{\partial^2 F_I}{\partial y^2}\,\mathrm{d}y + \frac{1}{2\pi}\int_0^{2\pi\gamma_0} \beta^2 \frac{\partial^2 F_{II}}{\partial y^2}\,\mathrm{d}y + \frac{2}{3}(3)^{1/4}\lambda_q \varepsilon^{3/2}[a + d_1(1+\gamma_0)] = 0 \tag{39}$$

For convenience we replace $[a + d_1(1+\gamma_0)]$ with e_1 in Eq. (41) below, by using Eqs. (36) and (37) to solve these perturbation equations of each order, and matching the regular solutions with the boundary layer solutions at each end of the shell, we obtain the asymptotic solutions. For the outer tube, they are

$$\begin{aligned} W_I = {} & \varepsilon^{3/2}\left[A_{00}^{(3/2)} - A_{00}^{(3/2)}\left(\alpha_{01}^{(3/2)}\cos\varphi\frac{\pi/2+x}{\sqrt{\varepsilon}} + \alpha_{10}^{(3/2)}\sin\varphi\frac{\pi/2+x}{\sqrt{\varepsilon}}\right)\exp\left(-\vartheta\frac{\pi/2+x}{\sqrt{\varepsilon}}\right)\right. \\ & \left. - A_{00}^{(3/2)}\left(\alpha_{01}^{(3/2)}\cos\varphi\frac{\pi/2-x}{\sqrt{\varepsilon}} + \alpha_{10}^{(3/2)}\sin\varphi\frac{\pi/2-x}{\sqrt{\varepsilon}}\right)\exp\left(-\vartheta\frac{\pi/2-x}{\sqrt{\varepsilon}}\right)\right] \\ & + \varepsilon^2[A_{11}^{(2)}\cos mx\cos ny] \\ & + \varepsilon^4[A_{00}^{(4)} + A_{11}^{(4)}\cos mx\cos ny + A_{20}^{(4)}\cos 2mx + A_{02}^{(4)}\cos 2ny] + O(\varepsilon^5) \end{aligned} \tag{40}$$

$$\begin{aligned} F_I = {} & -e_1 B_{00}^{(0)}\frac{y^2}{2} - (C_p + \beta^2 C_{00}^{(0)})\frac{x^2}{2} + \varepsilon^2\left[-e_1 B_{00}^{(2)}\frac{y^2}{2} - \beta^2 C_{00}^{(2)}\frac{x^2}{2} + B_{11}^{(2)}\cos mx\cos ny\right] \\ & + \varepsilon^{5/2}\left[A_{00}^{(3/2)}\left(\beta_{01}^{(5/2)}\cos\varphi\frac{\pi/2+x}{\sqrt{\varepsilon}} + \beta_{10}^{(5/2)}\sin\varphi\frac{\pi/2+x}{\sqrt{\varepsilon}}\right)\exp\left(-\vartheta\frac{\pi/2+x}{\sqrt{\varepsilon}}\right)\right. \\ & \left. + A_{00}^{(3/2)}\left(\beta_{01}^{(5/2)}\cos\varphi\frac{\pi/2-x}{\sqrt{\varepsilon}} + \beta_{10}^{(5/2)}\sin\varphi\frac{\pi/2-x}{\sqrt{\varepsilon}}\right)\exp\left(-\vartheta\frac{\pi/2-x}{\sqrt{\varepsilon}}\right)\right] \\ & + \varepsilon^4\left[-e_1 B_{00}^{(4)}\frac{y^2}{2} - \beta^2 C_{00}^{(4)}\frac{x^2}{2} + B_{20}^{(4)}\cos 2mx + B_{02}^{(4)}\cos 2ny\right] + O(\varepsilon^5) \end{aligned} \tag{41}$$

$$\Psi_{xI} = \varepsilon^2\left[\left(\varsigma_{01}^{(2)}\cos\varphi\frac{\pi/2+x}{\sqrt{\varepsilon}} + \varsigma_{10}^{(2)}\sin\varphi\frac{\pi/2+x}{\sqrt{\varepsilon}}\right)\exp\left(-\vartheta\frac{\pi/2+x}{\sqrt{\varepsilon}}\right)\right.$$
$$\left.+\left(\varsigma_{01}^{(2)}\cos\varphi\frac{\pi/2-x}{\sqrt{\varepsilon}} + \varsigma_{10}^{(2)}\sin\varphi\frac{\pi/2-x}{\sqrt{\varepsilon}}\right)\exp\left(-\vartheta\frac{\pi/2-x}{\sqrt{\varepsilon}}\right)\right]$$
$$+\varepsilon^3[C_{11}^{(3)}\sin mx\cos ny] + \varepsilon^5[C_{20}^{(5)}\sin 2mx] + O(\varepsilon^6) \tag{42}$$

$$\Psi_{yI} = \varepsilon^3[D_{11}^{(3)}\cos mx\sin ny] + \varepsilon^5[D_{02}^{(5)}\sin 2ny] + O(\varepsilon^6) \tag{43}$$

and for the inner tube it is just necessary to replace $-C_p$ in Eq. (41) with $+C_p$, and replace $A_{ik}^{(j)}, B_{ik}^{(j)}, C_{ik}^{(j)}$ and $D_{ik}^{(j)}$ in Eqs. (40)–(43) with $a_{ik}^{(j)}, b_{ik}^{(j)}, c_{ik}^{(j)}$ and $d_{ik}^{(j)}$, so that the asymptotic solutions W_{II}, F_{II}, Ψ_{xII} and Ψ_{yII} have a similar form.

Note that all of the coefficients in Eqs. (40)–(43) are related and can be expressed in terms of $A_{11}^{(2)}$, but for the sake of brevity the detailed expressions are not shown, whereas ϑ and φ are given in detail in Appendix A.

Because the end-shortening displacements of the outer and inner tubes are identical, upon substitution of F_I and F_{II} into Eqs. (32a) and (32b), we have

$$\chi_1 = \frac{1}{2B_1}\{[(B_2)^2 + 4B_1B_3]^{1/2} - B_2\} \tag{44}$$

where

$$B_1 = \frac{0.5\gamma_{24}^2 e_1 - \gamma_5}{\gamma_{24}^2(1+\gamma_0)}\frac{m^2}{n^2\beta^2 + 0.5e_1m^2} \tag{45a}$$

$$B_2 = \left(\frac{1}{\gamma_0} - 2B_1\right) + \frac{g_{08}}{C_0}[1 - B_1(1+\gamma_0)]$$
$$+\frac{\gamma_{14}m^2}{C_0}\left[\frac{\gamma_{24}m^2}{\gamma_0 g_{06}\mu_{11}}\left(\frac{1}{\gamma_0} - B_1(1+\gamma_0)\right) + C_p\frac{n^2\beta^2}{m^2}[1 + B_1(1-\gamma_0)] + \frac{2C_p\gamma_5}{\gamma_{24}^2(1+\gamma_0)}\right]\mu_{11}\varepsilon^{-2} \tag{45b}$$

$$B_3 = \frac{1}{\gamma_0} - B_1 \tag{45c}$$

Next, upon substitution of Eqs. (40)–(43) into the boundary condition (39) and into Eqs. (31) and (32c), the postbuckling equilibrium paths for the loading case (1) can be written as

$$\lambda_q = \frac{1}{4}(3)^{3/4}\varepsilon^{-3/2}[\lambda_q^{(0)} + \lambda_q^{(2)}(A_{11}^{(2)}\varepsilon^2)^2 + \cdots] \tag{46}$$

and

$$\delta_q = \delta_q^{(0)} - \delta_q^{(T)} + \delta_q^{(2)}(A_{11}^{(2)}\varepsilon^2)^2 + \cdots \tag{47}$$

It is noted that, in Eqs. (46) and (47), $\lambda_q^{(i)}$ and $\delta_q^{(i)}(i = 0, 2, \ldots)$ are related to the material properties and are all functions of temperature. Here $(A_{11}^{(2)}\varepsilon^2)$ is taken as the second perturbation parameter relating to the dimensionless maximum deflection. From Eq. (40), by taking $(x, y) = (m\pi, n\pi)$, one has

$$A_{11}^{(2)}\varepsilon^2 = W_m - \Theta_1 W_m^2 + \cdots \tag{48a}$$

where W_m is the dimensionless form of the maximum deflection of the outer tube that can be expressed as

$$W_m = \left[\varepsilon\frac{h}{[D_{11}^* D_{22}^* A_{11}^* A_{22}^*]^{1/4}}\frac{\overline{W}}{h} + \Theta_2\right] \tag{48b}$$

All symbols used in Eqs. (45)–(48) and Eqs. (55)–(58) below are also described in detail in Appendix A.

Case (2) high values of axial compression combined with relatively low external pressure. Let

$$\frac{\pi R_j^2 q}{P} = d_2 \tag{49a}$$

or

$$\frac{\frac{4}{3}(3)^{1/4}\lambda_q\varepsilon^{3/2}}{2\lambda_p\varepsilon}=2d_2 \tag{49b}$$

In this case, the boundary condition of Eq. (30d) becomes

$$\frac{1}{2\pi}\int_0^{2\pi}\beta^2\frac{\partial^2 F_I}{\partial y^2}\,\mathrm{d}y+\frac{1}{2\pi}\int_0^{2\pi\gamma_0}\beta^2\frac{\partial^2 F_{II}}{\partial y^2}\,\mathrm{d}y+2\lambda_p\varepsilon[(1+ad_2)+\gamma_0]=0 \tag{50}$$

Similarly, by taking $e_2=2d_2/(1+\gamma_0+ad_2)$ and using a singular perturbation procedure, the asymptotic solutions for the outer tube are obtained as

$$\begin{aligned}
W_I=\varepsilon&\left[A_{00}^{(1)}-A_{00}^{(1)}\left(\alpha_{01}^{(1)}\cos\varphi\frac{\pi/2+x}{\sqrt{\varepsilon}}+\alpha_{10}^{(1)}\sin\varphi\frac{\pi/2+x}{\sqrt{\varepsilon}}\right)\exp\left(-\vartheta\frac{\pi/2+x}{\sqrt{\varepsilon}}\right)\right.\\
&\left.-A_{00}^{(1)}\left(\alpha_{01}^{(1)}\cos\varphi\frac{\pi/2-x}{\sqrt{\varepsilon}}+\alpha_{10}^{(1)}\sin\varphi\frac{\pi/2-x}{\sqrt{\varepsilon}}\right)\exp\left(-\vartheta\frac{\pi/2-x}{\sqrt{\varepsilon}}\right)\right]\\
&+\varepsilon^2\left[A_{11}^{(2)}\cos mx\cos ny+A_{02}^{(2)}\cos 2ny\right.\\
&-(A_{02}^{(2)}\cos 2ny)\left(\alpha_{01}^{(1)}\cos\varphi\frac{\pi/2+x}{\sqrt{\varepsilon}}+\alpha_{10}^{(1)}\sin\varphi\frac{\pi/2+x}{\sqrt{\varepsilon}}\right)\exp\left(-\vartheta\frac{\pi/2+x}{\sqrt{\varepsilon}}\right)\\
&\left.-(A_{02}^{(2)}\cos 2ny)\left(\alpha_{01}^{(1)}\cos\varphi\frac{\pi/2-x}{\sqrt{\varepsilon}}+\alpha_{10}^{(1)}\sin\varphi\frac{\pi/2-x}{\sqrt{\varepsilon}}\right)\exp\left(-\vartheta\frac{\pi/2-x}{\sqrt{\varepsilon}}\right)\right]\\
&+\varepsilon^4\left[A_{00}^{(4)}+A_{11}^{(4)}\cos mx\cos ny+A_{20}^{(4)}\cos 2mx+A_{02}^{(4)}\cos 2ny\right.\\
&\left.+A_{13}^{(4)}\cos mx\cos 3ny+A_{04}^{(4)}\cos 4ny\right]+O(\varepsilon^6)
\end{aligned} \tag{51}$$

$$\begin{aligned}
F_I=&-B_{00}^{(0)}\frac{y^2}{2}-e_2\left(\beta^2B_{00}^{(0)}+\gamma_0\beta^2b_{00}^{(0)}\right)\frac{x^2}{2}-C_p\frac{x^2}{2}\\
&+\varepsilon^2\left[-B_{00}^{(2)}\frac{y^2}{2}-e_2\left(\beta^2B_{00}^{(2)}+\gamma_0\beta^2b_{00}^{(2)}\right)\frac{x^2}{2}+B_{11}^{(2)}\cos mx\cos ny\right.\\
&+A_{00}^{(1)}\left(\beta_{01}^{(2)}\cos\varphi\frac{\pi/2+x}{\sqrt{\varepsilon}}+\beta_{10}^{(2)}\sin\varphi\frac{\pi/2+x}{\sqrt{\varepsilon}}\right)\exp\left(-\vartheta\frac{\pi/2+x}{\sqrt{\varepsilon}}\right)\\
&\left.+A_{00}^{(1)}\left(\beta_{01}^{(2)}\cos\varphi\frac{\pi/2-x}{\sqrt{\varepsilon}}+\beta_{10}^{(2)}\sin\varphi\frac{\pi/2-x}{\sqrt{\varepsilon}}\right)\exp\left(-\vartheta\frac{\pi/2-x}{\sqrt{\varepsilon}}\right)\right]\\
&+\varepsilon^3\left[(A_{02}^{(2)}\cos 2ny)\left(\beta_{01}^{(3)}\cos\varphi\frac{\pi/2+x}{\sqrt{\varepsilon}}+\beta_{10}^{(3)}\sin\varphi\frac{\pi/2+x}{\sqrt{\varepsilon}}\right)\exp\left(-\vartheta\frac{\pi/2+x}{\sqrt{\varepsilon}}\right)\right.\\
&\left.+(A_{02}^{(2)}\cos 2ny)\left(\beta_{01}^{(3)}\cos\varphi\frac{\pi/2-x}{\sqrt{\varepsilon}}+\beta_{10}^{(3)}\sin\varphi\frac{\pi/2-x}{\sqrt{\varepsilon}}\right)\exp\left(-\vartheta\frac{\pi/2-x}{\sqrt{\varepsilon}}\right)\right]\\
&+\varepsilon^4\left[-B_{00}^{(4)}\frac{y^2}{2}-e_2(\beta^2B_{00}^{(4)}+\gamma_0\beta^2b_{00}^{(4)})\frac{x^2}{2}+B_{20}^{(4)}\cos 2mx+B_{02}^{(4)}\cos 2ny\right.\\
&\left.+B_{13}^{(4)}\cos mx\cos 3ny\right]+O(\varepsilon^6)
\end{aligned} \tag{52}$$

$$\begin{aligned}
\Psi_{xI}=\varepsilon^{3/2}&\left[A_{00}^{(1)}\left(\varsigma_{01}^{(3/2)}\cos\varphi\frac{\pi/2+x}{\sqrt{\varepsilon}}+\varsigma_{10}^{(3/2)}\sin\varphi\frac{\pi/2+x}{\sqrt{\varepsilon}}\right)\exp\left(-\vartheta\frac{\pi/2+x}{\sqrt{\varepsilon}}\right)\right.\\
&\left.+A_{00}^{(1)}\left(\varsigma_{01}^{(3/2)}\cos\varphi\frac{\pi/2-x}{\sqrt{\varepsilon}}+\varsigma_{10}^{(3/2)}\sin\varphi\frac{\pi/2-x}{\sqrt{\varepsilon}}\right)\exp\left(-\vartheta\frac{\pi/2-x}{\sqrt{\varepsilon}}\right)\right]\\
&+\varepsilon^{5/2}\left[(A_{02}^{(2)}\cos 2ny)\varsigma_{10}^{(5/2)}\sin\varphi\frac{\pi/2+x}{\sqrt{\varepsilon}}\exp\left(-\vartheta\frac{\pi/2+x}{\sqrt{\varepsilon}}\right)\right.\\
&\left.+(A_{02}^{(2)}\cos 2ny)\varsigma_{10}^{(5/2)}\sin\varphi\frac{\pi/2-x}{\sqrt{\varepsilon}}\exp\left(-\vartheta\frac{\pi/2-x}{\sqrt{\varepsilon}}\right)\right]+\varepsilon^3[C_{11}^{(3)}\sin mx\cos ny]\\
&+\varepsilon^5[C_{11}^{(5)}\sin mx\cos ny+C_{20}^{(5)}\sin 2mx+C_{13}^{(5)}\sin mx\cos 3ny]+O(\varepsilon^6)
\end{aligned} \tag{53}$$

$$\begin{aligned}\Psi_{yI} = \varepsilon^3 \Bigg[& D_{11}^{(3)} \cos mx \sin ny + D_{02}^{(3)} \sin 2ny \\ & - (A_{02}^{(2)} 2n\beta \sin 2ny) \left(\delta_{01}^{(3)} \cos\varphi \frac{\pi/2+x}{\sqrt{\varepsilon}} + \delta_{10}^{(3)} \sin\varphi \frac{\pi/2+x}{\sqrt{\varepsilon}} \right) \exp\left(-\vartheta \frac{\pi/2+x}{\sqrt{\varepsilon}} \right) \\ & - (A_{02}^{(2)} 2n\beta \sin 2ny) \left(\delta_{01}^{(3)} \cos\varphi \frac{\pi/2-x}{\sqrt{\varepsilon}} + \delta_{10}^{(3)} \sin\varphi \frac{\pi/2-x}{\sqrt{\varepsilon}} \right) \exp\left(-\vartheta \frac{\pi/2-x}{\sqrt{\varepsilon}} \right) \Bigg] \\ & + \varepsilon^5 [D_{11}^{(5)} \cos mx \sin ny + D_{02}^{(5)} \sin 2ny + D_{13}^{(5)} \cos mx \sin 3ny] + O(\varepsilon^6) \end{aligned} \tag{54}$$

and the asymptotic solutions for the inner tube can be obtained in the manner as described in the loading case (1). As a result, the axial stress resultants $\overline{N}_{xI}(=\overline{F}_{I,yy})$ and $\overline{N}_{xII}(=\overline{F}_{II,yy})$ are unequal, and can be obtained separately.

Upon substitution of F_I and F_{II} into Eqs. (32c) and (32d), the constant χ_1 can be given in the same form of Eq. (44), but now B_1, B_2 and B_3 are expressed as

$$B_1 = \frac{m^2}{m^2 + e_2 n^2 \beta^2} \tag{55a}$$

$$B_2 = \frac{1}{\gamma_0} - B_1 + \frac{g_{08}}{C_0}(1 - B_1) + \frac{\gamma_{14} m^2}{C_0} \left[\frac{\gamma_{24} m^2}{g_{06}} \left(\frac{1}{\gamma_0^2} - B_1 \right) + C_p \left(\frac{n^2\beta^2}{m^2}(B_1 + 1) + 2\frac{\gamma_5}{\gamma_{24}^2} \right) \mu_{11} \right] \varepsilon^{-2} \tag{55b}$$

$$B_3 = \frac{1}{\gamma_0} \tag{55c}$$

From Eqs. (45) and (55), it is evident that $\chi_1 < 1$, then inner tube has a lower amplitude than the outer tube. This follows from the fact that the outer tube is subjected to axial compression combined with both internal and external pressure, whereas the inner tube is subjected to the combined action of axial compression and external pressure.

Next, upon substitution of F_I and F_{II} into the boundary condition (50) and F_I and W_I into closed condition (31) and Eq. (32c), the postbuckling equilibrium paths for the loading case (2) can be written as

$$\lambda_p = \frac{1}{1 + ad_2 + \gamma_0} [\lambda_p^{(0)} - \lambda_p^{(2)} (A_{11}^{(2)} \varepsilon)^2 + \lambda_p^{(4)} (A_{11}^{(2)} \varepsilon)^4 + \cdots] \tag{56}$$

and

$$\delta_p = \delta_p^{(0)} - \delta_p^{(T)} + \delta_p^{(2)} (A_{11}^{(2)} \varepsilon)^2 + \delta_p^{(4)} (A_{11}^{(2)} \varepsilon)^4 + \cdots \tag{57}$$

In Eqs. (56) and (57), $\lambda_p^{(i)}$ and $\delta_p^{(i)} (i = 0, 2, \ldots)$ are also functions of temperature, and $(A_{11}^{(2)}\varepsilon)$ is taken as the second perturbation parameter in this case, and from Eq. (51) we have

$$A_{11}^{(2)} \varepsilon = W_m - \Theta_3 W_m^2 + \cdots \tag{58a}$$

and the dimensionless maximum deflection of the outer tube is written as

$$W_m = \left[\frac{h}{[D_{11}^* D_{22}^* A_{11}^* A_{22}^*]^{1/4}} \frac{\overline{W}}{h} + \Theta_4 \right] \tag{58b}$$

Eqs. (46)–(48) and Eqs. (56)–(58) are employed to obtain numerical results for full nonlinear postbuckling load–shortening and/or load–deflection curves of double-walled carbon nanotubes subjected to combined axial and radial loads in thermal environments, from which results for single-walled carbon nanotubes are obtained as a limiting case. Also, buckling under external pressure alone and buckling under axial compression alone follow as two limiting cases. By increasing d_1 and d_2, respectively, the interaction curve of a double-walled carbon nanotube under combined loading can be constructed with these two lines. Note that since $d_2 = 1/d_1$, only one load-proportional parameter should be determined in advance. The initial buckling load for a perfect double-walled carbon nanotube can readily be obtained numerically, by setting $\overline{W}^*/t = 0$ (or $\mu = 0$), while taking $\overline{W}/t = 0$ (note that $W_m \neq 0$). In this case, the minimum buckling load is determined by considering Eq. (46) or (56) for various values of the buckling mode (m,n), which determine the number

of half-waves in the X-direction and of full waves in the Y-direction. Note that because of Eqs. (40) and (51), the prebuckling deformation of the tube is nonlinear.

4. Numerical results and discussions

Numerical results are presented in this section for double-walled carbon nanotubes with temperature dependent material properties and initial point defects. The key issue is first to determine the material properties and effective wall thickness of a single-walled carbon nanotube.

The molecular dynamics simulations are first carried out. We use the many-body reactive empirical bond order potential developed by Brenner (Brenner, 1990; Brenner et al., 2002) to describe the interaction between carbon atoms. System temperature conversion is carried out by the Nose-Hoover feedback thermostat (Hoover, 1985). In the frame work of MD simulation, the nanotube can be considered as a congeries of individual atoms. The integration of Newtonian dynamics function is used to determine the variation of the instantaneous location and velocity of each atom. The perfect single-walled carbon nanotubes subjected to axial compression and torsion are simulated under temperature varying from 300 to 1500 K. Fixed boundary condition is assumed to be at one end of the tube, and axial compressive force P_x or torque T_s is applied on the other end with the appropriate constraints (Zhang and Shen, 2006).

From MD simulation results the effective material properties for armchair (8, 8) single-walled carbon nanotubes can be chosen properly and then the results for its alternative multi-walled carbon nanotubes can be obtained numerically in the manner similar to that of Tu and Ou-Yang (2002). Typical results are listed in Table 1 for (8, 8) carbon nanotubes with $L = 6.309$ nm, $R_{\text{in}} = 0.546$ nm, and $h = 0.0623$ nm under thermal environmental conditions $T = 300$, 800 and 1500 K, in which N is the layer number of the multi-walled carbon nanotube and R_{in} is the inmost radius of the tube, and the intertube distance is taken to be 0.34 nm. It is noted that the effective Young's modulus does not reflect the physics change in the true lattice rigidity but just a choice of the cross section. HereR_{in} remains constant, so that the outmost radius of the tube increases as the number of layers N increases. From Table 1 we confirm that the material properties are dependent on the temperature and the layer number, and the effective Young's modulus E_{11} reduces to 1.1 TPa when $N > 20$.

We now examine the effect of material properties and effective wall thickness on the postbuckling behavior of an armchair (8, 8) single-walled carbon nanotube. Four cases, i.e. (1) $E = 5.5$ TPa, $\nu = 0.19$, $h = 0.066$ nm (Yakobson et al., 1996), (2) $E = 4.84$ TPa, $\nu = 0.19$, $h = 0.075$ nm (Pantano et al., 2004), (3) $E = 5.1$ TPa, $\nu = 0.24$, $h = 0.074$ nm (Zhou et al., 2000), and (4) $E = 1.28$ TPa, $\nu = 0.25$, $h = 0.154$ nm (Liew et al., 2004), are considered. The postbuckling load–shortening curves are calculated and are compared in Fig. 2 with our MD simulation results at $T = 300$ K. It can be seen that the results of case (1) agree reasonably well with MD simulations. In contrast, the buckling load is higher and the critical strain is much larger than our MD simulation results when $E = 1.28$ TPa, $\nu = 0.25$ and $h = 0.154$ nm. From Fig. 2 we believe that the postbuckling behavior of a single-walled carbon nanotube is sensitive to the material properties and effective wall thickness, and the wide used value of 0.34 nm for tube wall thickness is thoroughly inappropriate to single-walled carbon nanotubes.

Table 1
Temperature-dependent material properties E_{11} (TPa) and G_{12} (TPa) for an armchair multi-walled carbon nanotube ($L = 6.309$ nm, $R_{in} = 0.546$ nm, $h = 0.0623$ nm and $\nu_{12} = 0.167$)

N	1	2	3	4	5	10	20	50	100
$T = 300$ K, $\alpha_{11} = 2.7749 \times 10^{-6}$/K, $\alpha_{22} = 6.0436 \times 10^{-6}$/K									
E_{11}	6.3401	1.9636	1.5963	1.4598	1.3885	1.2650	1.2112	1.1810	1.1713
G_{12}	2.1257	0.6584	0.5352	0.4894	0.4655	0.4241	0.4061	0.3960	0.3927
$T = 800$ K, $\alpha_{11} = 4.5016 \times 10^{-6}$/K, $\alpha_{22} = 4.4885 \times 10^{-6}$/K									
E_{11}	5.9804	1.8522	1.5058	1.3770	1.3098	1.1933	1.1425	1.1140	1.1048
G_{12}	2.1417	0.6633	0.5392	0.4931	0.4690	0.4273	0.4091	0.3989	0.3957
$T = 1500$ K, $\alpha_{11} = 5.1603 \times 10^{-6}$/K, $\alpha_{22} = 5.0269 \times 10^{-6}$/K									
E_{11}	5.5534	1.7200	1.3983	1.2787	1.2162	1.1081	1.0609	1.0345	1.0259
G_{12}	2.1192	0.6563	0.5336	0.4879	0.4641	0.4228	0.4048	0.3948	0.3915

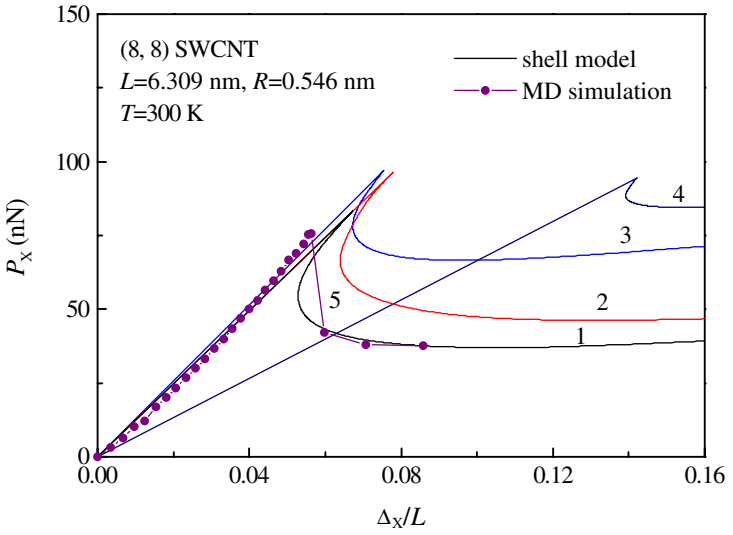

1: E=5.5 TPa, h=0.066 nm, ν=0.19,
2: E=4.84 TPa, h=0.075 nm, ν=0.19
3: E=5.1 TPa, h=0.074 nm, ν=0.24
4: E=1.28 TPa, h=0.154 nm, ν=0.25
5: Present MD simulation

Fig. 2. Comparisons of postbuckling behavior for a (8, 8) single-walled carbon nanotube under axial compression.

Fig. 3 gives the postbuckling load–shortening curves for (8, 8) single-walled carbon nanotubes subjected to axial compression under thermal environmental conditions, and the results are compared with the MD simulation results at $T = 300$ and 800 K. The temperature-dependent material properties are used in the present example, e.g. $E_{11} = E_{22} = 5.9804$ TPa, $G_{12} = G_{13} = G_{23} = 2.1417$ TPa, $\nu_{12} = 0.167$, $\alpha_{11} = 4.5016 \times 10^{-6}$/K, $\alpha_{22} = 4.4885 \times 10^{-6}$/K at $T = 800$ K, as given in Table 1 for a single-walled carbon nanotube with $N = 1$. Some numerical results are also presented in Table 2 to enable easy comparisons by others in the future. It

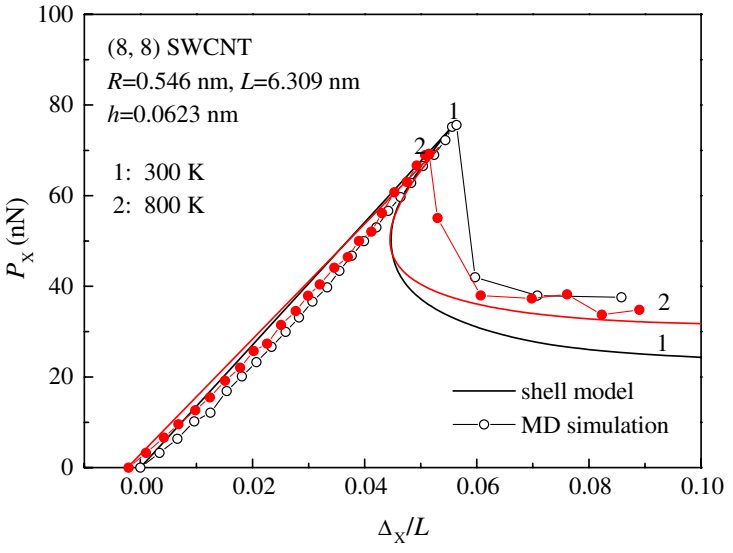

Fig. 3. Comparisons of postbuckling behavior for a (8,8) single-walled carbon nanotube under axial compression in thermal environments.

Table 2
Buckling behavior for single-walled carbon nanotubes subjected to axial compression in thermal environments ($L = 6.309$ nm, $R = 0.546$ nm, and $h = 0.0623$ nm)

	(8, 8)-tube		
	Initial extension strain	Buckling load P_{cr} (nN)	Critical strain
T = 300 K			
MD simulation	0.0	75.5836	0.0564
Shell model (HSDST)	0.0	75.6182	0.0559
Shell model (CST)	0.0	78.4134	0.0580
T = 800 K			
MD simulation	−0.0021	69.2429	0.0515
Shell model (HSDST)	−0.0023	70.5575	0.0532
Shell model (CST)	−0.0023	73.0217	0.0552

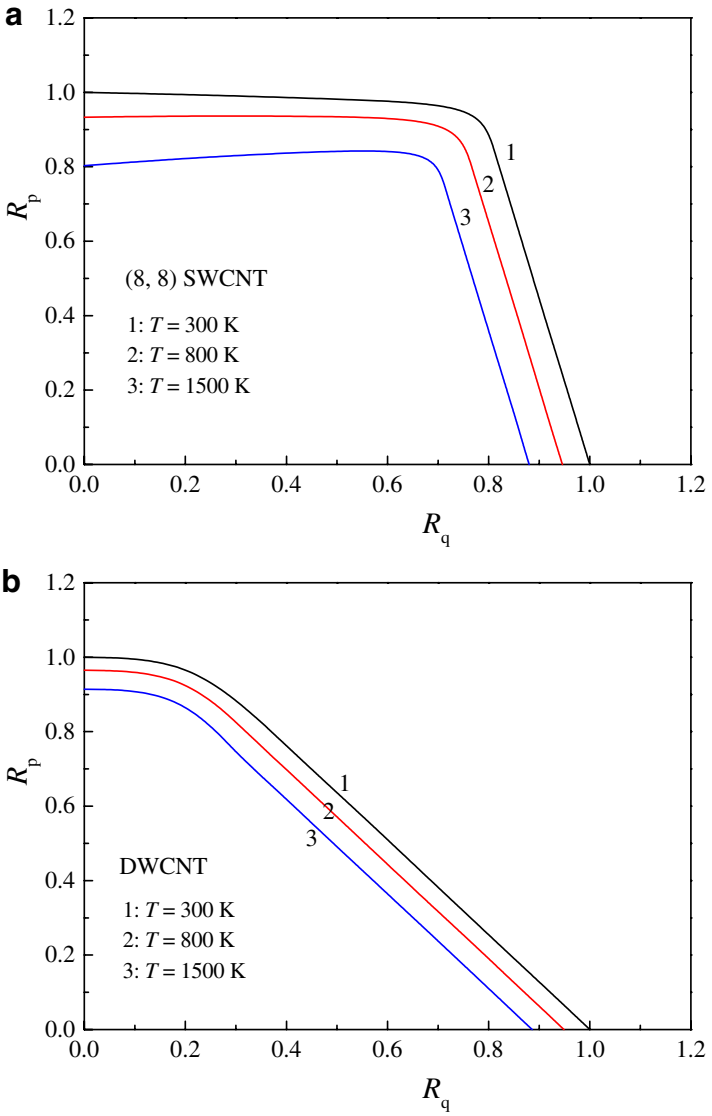

Fig. 4. Interaction buckling curves for single- and double-walled carbon nanotubes subjected to combined axial and radial loads in three different sets of thermal environmental conditions: (a) SWCNT; (b) DWCNT.

is found that an initial extension occurs as the temperature increases and the buckling loads are reduced with increases in temperature, which confirming the finding of Ni et al. (2002) for an empty nanotube. It can be seen that the HSDST results agree well with the MD simulation results when the material properties are properly chosen. In contrast, the buckling loads from classical shell theory (CST) are, respectively, about +3.7% and

Table 3
Buckling loads for a double-walled carbon nanotube subjected to axial compression alone or lateral pressure alone in thermal environments ($L = 6.309$ nm, $R_I = 0.886$ nm, $R_{II} = 0.546$ nm, and $h = 0.0623$ nm)

T	P_x (nN)	q (GPa)
300	29.4746	0.5915
800	28.4430	0.5613
1500	26.9398	0.5241

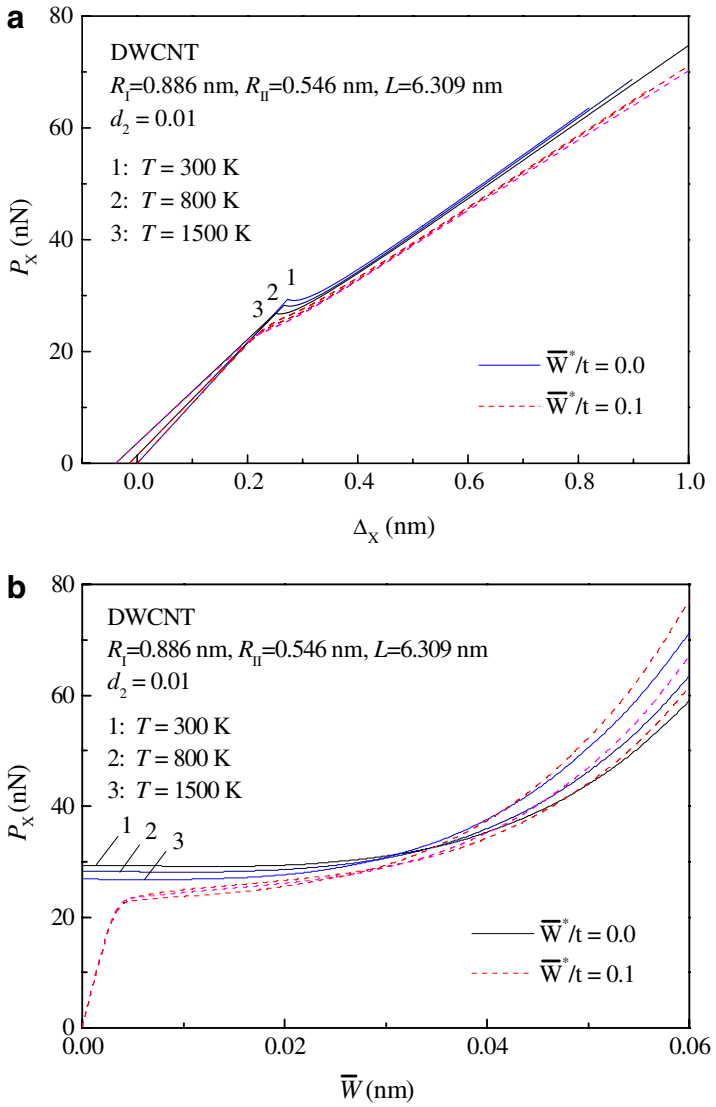

Fig. 5. The effect of temperature rise on the postbuckling behavior for a pressure-loaded double-walled carbon nanotube subjected to axial compression: (a) load–shortening; (b) load–deflection.

+5.5% higher than those of MD simulations under thermal environmental conditions $T = 300$ and 800 K. This is because in the present example the shell radius-to-thickness ratio ($R/h = 8.76$) is much smaller than 20, and in such a case the transverse shear deformation should be taken into account.

Fig. 4 shows the effects of temperature rise on the interaction buckling curves of (8, 8) single-walled carbon nanotube and its alternative double-walled carbon nanotube under combined loading cases in thermal environmental conditions $T = 300$, 800 and 1500 K, in which $R_q = q/q_{cr}$ and $R_p = P_x/P_{cr}$, where q_{cr} and P_{cr} are the critical buckling loads for the tube under radial pressure alone or axial compression alone at $T = 300$ K, as given in Table 3. For the sake of illustration, we consider the initial interlayer spacing between the inner and outer tube is 0.34 nm, so that the geometric parameters of the double-walled carbon nanotube are: $L = 6.309$ nm, $R_I = 0.886$ nm, $R_{II} = 0.546$ nm and each tube has the same thickness $h = 0.0623$ nm. As mentioned before, in such a case the initial pressure p_0 is zero or $C_1 = 0$. By taking $\varepsilon_0 = 2.39$ meV and $\sigma_0 = 0.341$ nm, from Eq. (1), we have the van der Waals interaction constant $C = 69.6474$ GPa/nm, which lies between 61.9917 GPa/nm and 99.1867 GPa/nm as previously given in Ru (2001b), Wang et al. (2003b). From

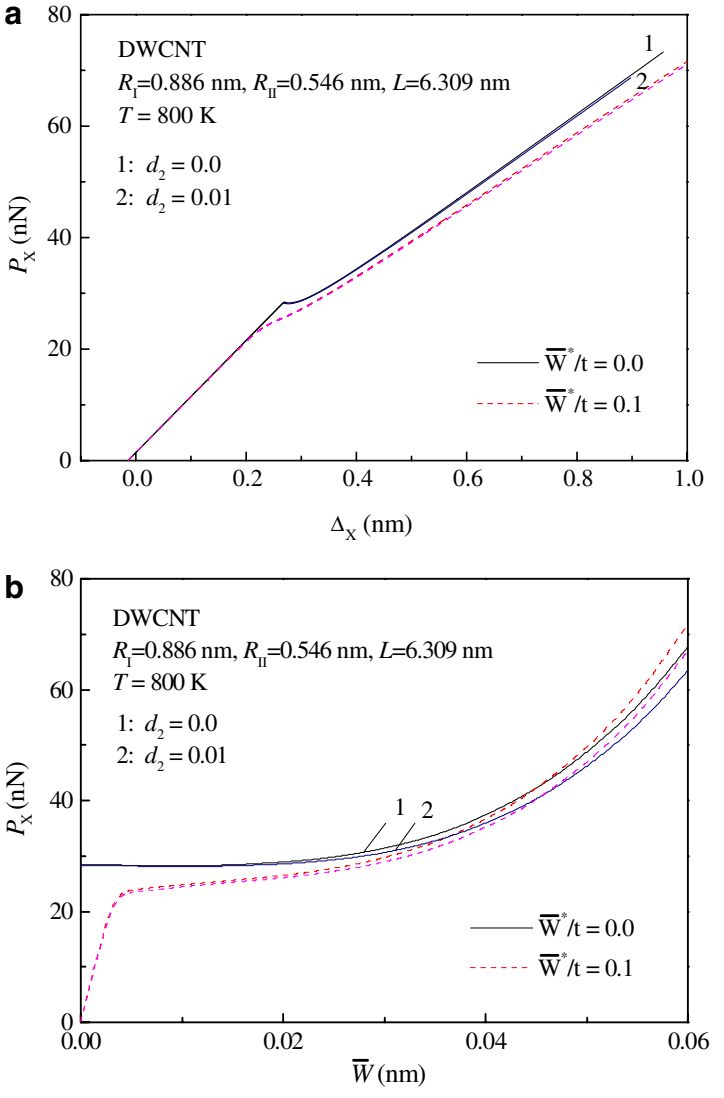

Fig. 6. Postbuckling behavior of a pressure-loaded double-walled carbon nanotube subjected to axial compression in thermal environmental condition $T = 800$ K: (a) load–shortening; (b) load–deflection.

Fig. 4 it can be seen that the shape of the interaction buckling curves for single-walled and double-walled carbon nanotubes are quite different, and the temperature rise has a significant effect on the shape of the interaction buckling curves.

Fig. 5 gives the postbuckling load–shortening and load–deflection curves of a double-walled carbon nanotube under combined loading case (2) with the load-proportional parameter $d_2 = 0.01$ and under thermal environmental conditions $T = 300$, 800 and 1500 K. The temperature dependent material properties are used in the present example, e.g. $E_{11} = E_{22} = 1.8522$ TPa, $G_{12} = G_{13} = G_{23} = 0.6633$ TPa, $v_{12} = 0.167$, $\alpha_{11} = 4.5016 \times 10^{-6}$/K, $\alpha_{22} = 4.4885 \times 10^{-6}$/K at $T = 800$ K, as given in Table 1 for a double-walled carbon nanotube with $N = 2$. For these three thermal environmental cases $\chi_1 = 0.4909$, 0.4998 and 0.5137, respectively, and $\overline{W}_I - \overline{W}_{II}$ is definitely less than 0.425 nm in the postbuckling region, so that the linear function assumption for the van der Waals interaction force is reasonable. It is found that an initial extension occurs as the temperature increases. It can be seen that the buckling loads and postbuckling loads in the initial postbuckling region are both reduced with increases in temperature, but the effect of temperature changes is rather small.

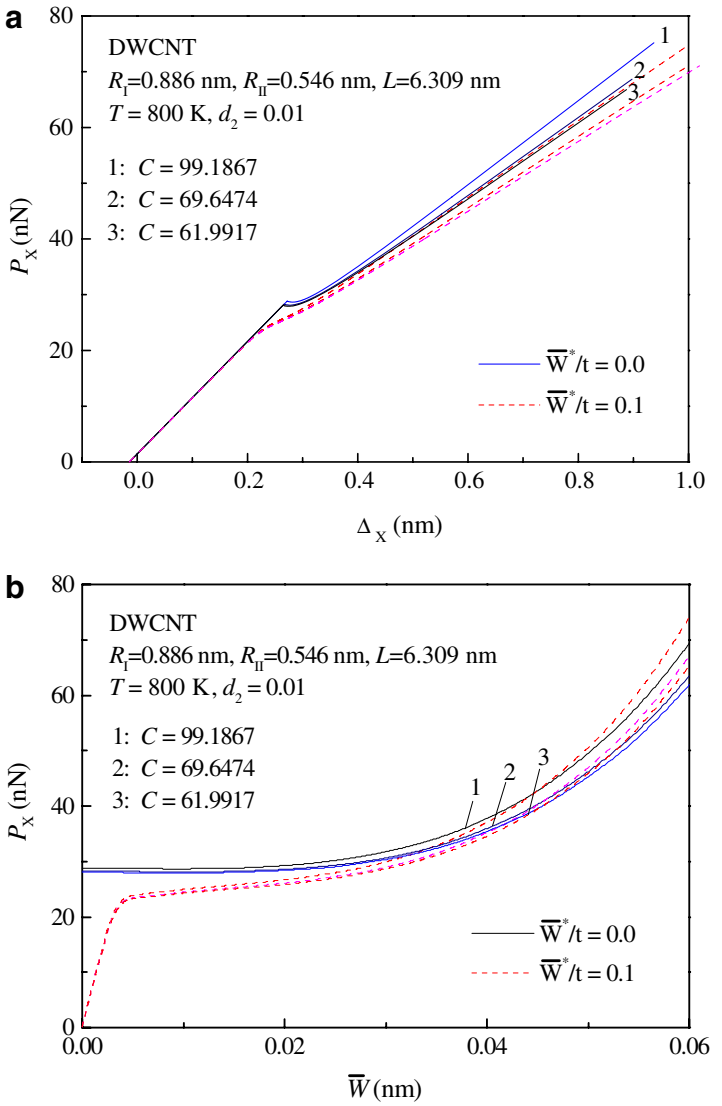

Fig. 7. Comparisons of postbuckling behavior for pressure-loaded double-walled carbon nanotubes with different values of the van der Waals interaction constant C subjected to axial compression in thermal environmental condition $T = 800$ K: (a) load–shortening; (b) load–deflection.

Fig. 6 gives the postbuckling load–shortening and load–deflection curves of a double-walled carbon nanotube under combined loading case (2) with the load-proportional parameter $d_2 = 0.0$ and 0.01 at $T = 800$ K. It can be seen that, for the perfect carbon nanotube ($\overline{W}^*/t = 0$), only a very weak "snap-through" phenomenon occurs in the postbuckling region. It can also be seen that an increase in load is usually required to obtain an increase in displacement when an initial defect is existed. This phenomenon is very similar to that observed in the buckling experiment reported in Waters et al. (2004, 2005). In such a case, the postbuckling path is stable and the double-walled carbon nanotube is virtually imperfection–insensitive.

Fig. 7 compares the postbuckling load–shortening and load–deflection curves for a double-walled carbon nanotube under combined loading case (2) with the load-proportional parameter $d_2 = 0.01$ and under three different values of C in thermal environmental condition $T = 800$ K. The results show that the van der Waals interaction constant C only has a very small effect on the buckling load of carbon nanotubes, and the effect becomes pronounced when the deflection is sufficiently large.

Figs. 8 and 9 show, respectively, the effects of temperature rise and initial axial compression on the postbuckling behavior of the same double-walled carbon nanotube analogous to the cases of Figs. 5 and 6, but

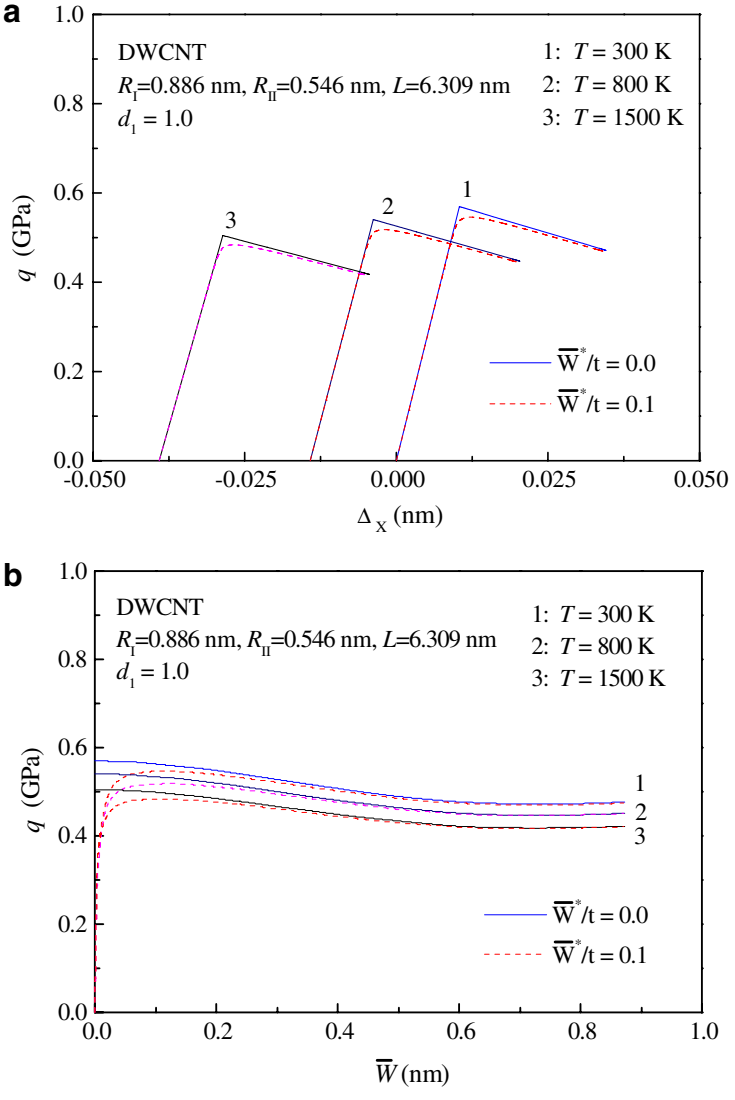

Fig. 8. The effect of temperature rise on the postbuckling behavior for an axially-loaded double-walled carbon nanotube subjected to external pressure: (a) load–shortening; (b) load–deflection.

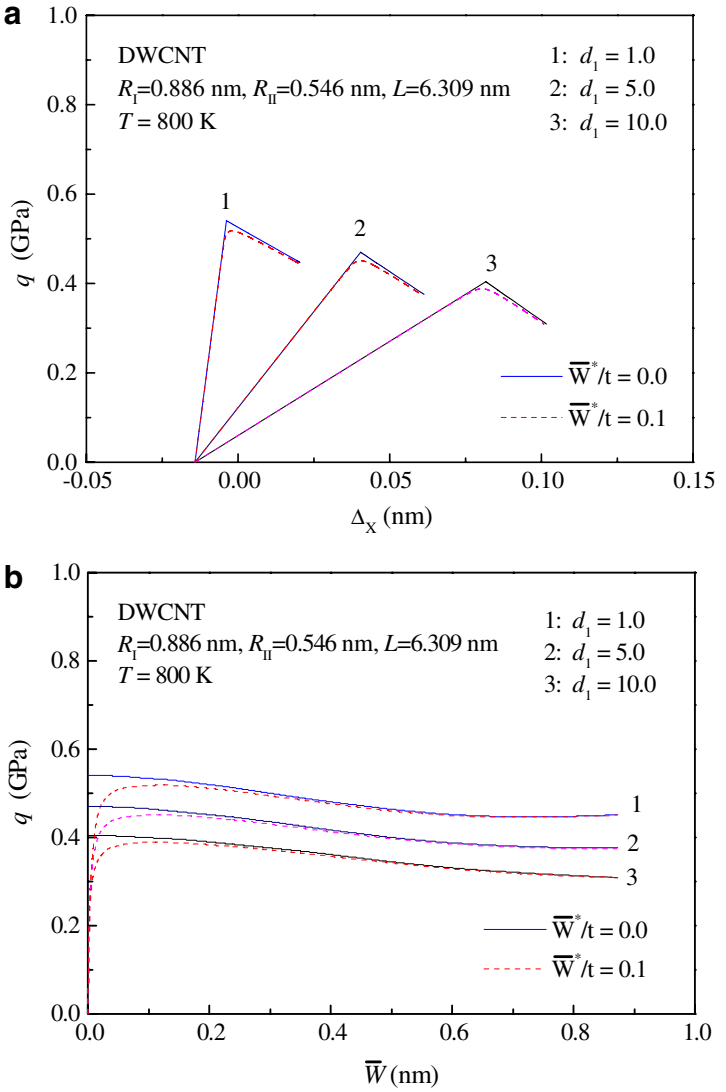

Fig. 9. Postbuckling behavior of an axially-loaded double-walled carbon nanotube subjected to external pressure in thermal environmental condition $T = 800$ K: (a) load–shortening; (b) load–deflection.

under combined loading case (1) with load-proportional parameter $d_1 = 1.0$, 5.0 and 10.0. Now for these three thermal environmental cases $\chi_1 = 0.9831$, 0.9839 and 0.9850, respectively, and $\overline{W}_I - \overline{W}_{II}$ is much less than 0.425 nm. It can be seen that the double-walled carbon nanotube has an unstable postbuckling behavior when the external pressure is relatively high. This conclusion is consistent with that of Shen (2004).

The postbuckling load–shortening and load–deflection curves for imperfect double-walled carbon nanotubes have also been plotted in Figs. 5–9, in which $\overline{W}^*/t$ means the dimensionless form of the maximum initial geometric imperfection of the tube. The local imperfection parameters are taken to be $C_1/L = 0.01$ and $C_2/R_I = 0.1$.

5. Conclusion

The results presented provide a framework for the postbuckling prediction of double-walled carbon nanotubes subjected to combined axial and radial mechanical loads in thermal environments based on a continuum shear deformable shell model. Temperature-dependent material properties and initial point defects are both

taken into account. The results reveal that temperature change only has a small effect on the postbuckling behavior of double-walled carbon nanotubes. At the conclusion of this work, we believe that the continuum shear deformable shell model can predict the postbuckling response of double-walled and/or multi-walled carbon nanotubes when the material properties and effective wall thickness are properly given, and we now know two different kinds of postbuckling behaviors of double-walled carbon nanotubes. The double-walled carbon nanotube has an unstable postbuckling path under combined loading case (1), and the structure is imperfection–sensitive. In contrast, the double-walled carbon nanotube has a very weak "snap-through" postbuckling path under combined loading case (2), and the structure is virtually imperfection–insensitive.

Acknowledgement

This work is supported in part by the National Natural Science Foundation of China under Grant 50375091. The authors are grateful for this financial support.

Appendix A

In Eqs. (45)–(48)

$$\Theta_1 = \left[\frac{1}{8}n^2\beta^2\mu_{12} + \frac{1}{8}n^2\beta^2\mu_{11}\frac{g_{06}\mu_{12} + 8m^4\mu_{11}}{\Delta_2} - \frac{1}{4}\mu_{11}\frac{m^4(n^2\beta^2 + 0.5e_1m^2)}{\Delta_1}\frac{\mu_{11}}{\mu_{02}} + \frac{1}{\gamma_{24}}\left(1 - \gamma_5\frac{0.5\gamma_{24}^2e_1 + \gamma_0\gamma_5}{\gamma_{24}^2(1+\gamma_0)}\right)\lambda_q^{(2)}\right] \tag{A.1a}$$

$$\Theta_2 = \frac{1}{\gamma_{24}}[(\gamma_{T2} - \gamma_5\gamma_{T1})\Delta T]\varepsilon - \frac{C_p}{\gamma_{24}}\left(1 - 2\frac{\gamma_5^2}{\gamma_{24}^2}\frac{\gamma_0}{1+\gamma_0}\right) - \frac{1}{\gamma_{24}}\left(1 - \gamma_5\frac{0.5\gamma_{24}^2e_1 + \gamma_0\gamma_5}{\gamma_{24}^2(1+\gamma_0)}\right)\lambda_q^{(0)} \tag{A.1b}$$

$$\lambda_q^{(0)} = \frac{m^2}{(n^2\beta^2 + 0.5e_1m^2)}\left\{\left[\frac{\gamma_{24}m^2}{g_{06}\mu_{11}}\left(1 + \frac{1}{\gamma_0}\right) - C_p\frac{n^2\beta^2}{m^2}(1-\gamma_0)\right] + \frac{1}{\gamma_{14}m^2\mu_{11}}\left[g_{08}(1+\gamma_0) - C_0(1-\chi_1)\left(\frac{1}{\chi_1} - 1\right)\right]\varepsilon^2\right\} \tag{A.2a}$$

$$\lambda_q^{(2)} = \frac{m^2}{(n^2\beta^2 + 0.5e_1m^2)}\left\{\frac{1}{16\gamma_{24}}m^2(1+\chi_1^2\gamma_0)\mu_{12} + \frac{\gamma_{24}m^6n^2\beta^2}{2g_{06}}\frac{(n^2\beta^2 + 0.5e_1m^2)}{m^2}\left[\frac{\mu_{144} + \mu_{244}g_{10}}{\Delta_1\mu_{02}}\right] - \frac{1}{4}\frac{\gamma_{24}n^4\beta^4}{g_{06}m^2}\left[\frac{\Delta_3}{\Delta_2} + \chi_1^2\frac{\gamma_0\gamma_{24}\Delta_3'}{(\gamma_{24} - 4n^2\beta^2\gamma_0^2C_p\mu_{20})g_{06}\mu_{11} - 4m^4\gamma_{24}\mu_{20}}\right]\right\} \tag{A.2b}$$

$$\delta_q^{(0)} = \frac{1}{\gamma_{24}}\left[\frac{0.5\gamma_{24}^2e_1 - \gamma_5}{1+\gamma_0} + \frac{\gamma_5}{\pi\vartheta}\left(1 - \frac{\gamma_5}{\gamma_{24}^2}\frac{0.5\gamma_{24}^2e_1 + \gamma_0\gamma_5}{1+\gamma_0}\right)\varepsilon^{1/2}\right]\lambda_q - \frac{(3)^{3/4}}{4}\frac{C_p\gamma_5}{\gamma_{24}}\left[\frac{1-\gamma_0}{1+\gamma_0} - \frac{1}{\pi\vartheta}\left(1 - 2\frac{\gamma_5^2}{\gamma_{24}^2}\frac{\gamma_0}{1+\gamma_0}\right)\varepsilon^{1/2}\right]\varepsilon^{-3/2} \tag{A.3a}$$

$$\delta_q^{(T)} = \frac{(3)^{3/4}}{4\gamma_{24}}\varepsilon^{-1/2}\left[(\gamma_{24}^2\gamma_{T1} - \gamma_5\gamma_{T2}) + \frac{\gamma_5}{\pi\vartheta}(\gamma_{T2} - \gamma_5\gamma_{T1})\varepsilon^{1/2}\right]\Delta T \tag{A.3b}$$

$$\delta_q^{(2)} = \frac{(3)^{3/4}}{32}m^2\mu_{12}\varepsilon^{-3/2} \tag{A.3c}$$

in the above equations

$$\begin{aligned}
\Delta_1 &= \left(\frac{1+\gamma_0}{\gamma_0}\right)m^4 + \frac{1}{\gamma_{24}}C_p(\gamma_0 n^2\beta^2 + 0.5e_1m^2)g_{06}\mu_{11}\\
\Delta_2 &= \left[1 + 4n^2\beta^2\frac{C_p}{\gamma_{24}}\left(\frac{\gamma_0 n^2\beta^2 + 0.5e_1m^2}{n^2\beta^2 + 0.5e_1m^2}\right)\mu_{20}\right]g_{06}\mu_{11} - 4m^4\frac{0.5e_1m^2\gamma_0 - n^2\beta^2}{\gamma_0(n^2\beta^2 + 0.5e_1m^2)}\mu_{20}\\
\Delta_3 &= \left[\left(\mu_{122} + \frac{0.5e_1m^2\gamma_0 - n^2\beta^2}{\gamma_0(n^2\beta^2 + 0.5e_1m^2)}\mu_{12}\mu_{20}\right)m^4 \quad - \frac{C_p}{\gamma_{24}}\left(\frac{\gamma_0 n^2\beta^2 + 0.5e_1m^2}{n^2\beta^2 + 0.5e_1m^2}\right)n^2\beta^2 g_{06}\mu_{123}\right]g_{06} + 8m^8\mu_{124}\\
\Delta_3' &= \left[(\mu_{122} + \mu_{12}\mu_{20})m^4 + \frac{C_p}{\gamma_{24}}n^2\beta^2\gamma_0^2 g_{06}\mu_{123}\right]g_{06} + 8m^8\mu_{124}
\end{aligned} \tag{A.4}$$

and in Eqs. (55)–(58)

$$\Theta_3 = \left[\gamma_{14}\gamma_{24}m^4n^2\beta^2\frac{g_{21}}{g_{06}}\varepsilon^{-1} + 2\frac{\gamma_5}{\gamma_{24}}\lambda_B^{(2)} - 2\frac{e_2}{\gamma_{24}}\lambda_p^{(2)}\right] \tag{A.5a}$$

$$\Theta_4 = \frac{1}{\gamma_{24}}[2\gamma_5\lambda_B^{(0)} - 2e_2\lambda_p^{(0)} - C_p\varepsilon^{-1}] + \frac{1}{\gamma_{24}}(\gamma_{T2} - \gamma_5\gamma_{T1})\Delta T \tag{A.5b}$$

$$\lambda_p^{(i)} = \frac{1}{1 + ad_2 + \gamma_0}[\lambda_B^{(i)} + \gamma_0\lambda_b^{(i)}] \quad (i = 0, 2, 4) \tag{A.6}$$

where

$$\lambda_B^{(0)} = \frac{B_1}{2}\left\{\left[\frac{\gamma_{24}m^2}{g_{06}\mu_{11}} - C_p\frac{n^2\beta^2}{m^2}\right]\varepsilon^{-1} + \frac{1}{\gamma_{24}m^2\mu_{11}}[g_{08} - C_0(\chi_1 - 1)]\varepsilon\right\} \tag{A.7a}$$

$$\begin{aligned}
\lambda_B^{(2)} = \frac{B_1}{2}\Bigg\{&\frac{4\gamma_{14}\gamma_{24}^2m^6n^4\beta^4}{g_{06}^2\mu_{11}}g_{21}\varepsilon^{-1} - \frac{1}{16\gamma_{24}}m^2\mu_{12}\varepsilon\\
&+ \frac{\gamma_{24}n^4\beta^4}{4m^2g_{06}}\frac{(\gamma_{24}m^4\tilde{\mu}_{122} - n^2\beta^2C_pg_{06}\tilde{\mu}_{123})g_{06} + 8m^8\gamma_{24}\mu_{124}}{(\gamma_{24} + 4n^2\beta^2C_pB_1\mu_{20})g_{06}\mu_{11} - 4m^4\gamma_{24}B_1\mu_{20}}\varepsilon\\
&-2\gamma_{24}\frac{m^2n^4\beta^4}{g_{06}\mu_{11}}C_0\chi_1(g_{21} - \gamma_0g_{22}\mu_{11})\varepsilon\Bigg\}
\end{aligned} \tag{A.7b}$$

$$\begin{aligned}
\lambda_B^{(4)} = \frac{B_1}{2}\Bigg\{&\frac{4\gamma_{14}^2\gamma_{24}^3m^{10}n^8\beta^8}{g_{06}^3}\left[\frac{[\gamma_{24}m^4(1+B_{13}) + n^2\beta^2C_pB_{113}g_{06}\mu_{11}](g_{136} + g_{06}\mu_{11})\mu_{13}}{\gamma_{24}m^4(B_{13}g_{136}\mu_{13} - g_{06}\mu_{11}) + n^2\beta^2C_pB_{113}g_{136}g_{06}\mu_{11}\mu_{13}}\frac{g_{21}^2}{\mu_{11}}\right]\\
&+ g_{06}\left[\frac{\gamma_{24}m^4[2 + (1+B_{13})\mu_{13}] - n^2\beta^2C_pB_{113}(g_{136} - g_{06}\mu_{11})\mu_{13}}{\gamma_{24}m^4(B_{13}g_{136}\mu_{13} - g_{06}\mu_{11}) + n^2\beta^2C_pB_{113}g_{136}g_{06}\mu_{11}\mu_{13}}g_{21}g_{23}\right.\\
&\left.+\frac{2\gamma_{24}m^4(1+\mu_{13}) + 8n^2\beta^2C_p\gamma_0^2(g_{136} - g_{06}\mu_{11})\mu_{13}}{\gamma_{24}m^4(g_{136}\mu_{13} - g_{06}\mu_{11}) - 8n^2\beta^2C_p\gamma_0^2g_{136}g_{06}\mu_{11}\mu_{13}}C_0\gamma_0g_{22}g_{20}\right]\mu_{144}\Bigg\}\varepsilon^{-1}
\end{aligned} \tag{A.7c}$$

$$\lambda_b^{(0)} = \frac{B_1}{2}\left\{\left[\frac{\gamma_{24}m^2}{\gamma_0^2g_{06}\mu_{11}} + C_p\frac{n^2\beta^2}{m^2}\right]\varepsilon^{-1} + \frac{1}{\gamma_{24}m^2\mu_{11}}\left[g_{08} - C_0\frac{(1-\chi_1)}{\gamma_0\chi_1}\right]\varepsilon\right\} \tag{A.8a}$$

$$\begin{aligned}
\lambda_b^{(2)} = \frac{B_1}{2}\Bigg\{&\frac{4\gamma_{14}\gamma_{24}^2m^6n^4\beta^4}{\gamma_0g_{06}^2\mu_{11}}g_{22}\varepsilon^{-1} - \frac{1}{16\gamma_{24}}m^2\chi_1^2\mu_{12}\varepsilon\\
&+ \frac{\gamma_{24}n^4\beta^4}{4m^2g_{06}}\frac{(\gamma_{24}m^4\mu_{122} + n^2\beta^2\gamma_0^2C_pg_{06}\mu_{123})g_{06} + 8m^8\gamma_{24}\mu_{124}}{(\gamma_{24} - 4n^2\beta^2\gamma_0^2C_p\mu_{20})g_{06}\mu_{11} - 4m^4\gamma_{24}\mu_{20}}\chi_1^2\varepsilon\\
&+2\frac{\gamma_{24}m^2n^4\beta^4}{\gamma_0\chi_1g_{06}\mu_{11}}C_0(g_{21}\mu_{11} - \gamma_0g_{22})\varepsilon\Bigg\}
\end{aligned} \tag{A.8b}$$

$$\lambda_b^{(4)} = \frac{B_1}{2}\left\{\frac{4\gamma_{14}^2\gamma_{24}^3 m^{10}n^8\beta^8}{g_{06}^3}\left[\frac{(2\gamma_{24}m^4 - 8n^2\beta^2\gamma_0^2 C_p g_{06}\mu_{11}(g_{136}+g_{06}\mu_{11})\mu_{13}}{\gamma_{24}m^4(g_{136}\mu_{13}-g_{06}\mu_{11}) - 8n^2\beta^2\gamma_0^2 C_p g_{136}g_{06}\mu_{11}\mu_{13}}\frac{g_{22}^2}{\mu_{11}}\right]\right.$$
$$+\frac{g_{06}}{\gamma_0}\left[\frac{\gamma_{24}m^4[2+(1+B_{13})\mu_{13}] - n^2\beta^2 C_p B_{113}(g_{136}-g_{06}\mu_{11})\mu_{13}}{\gamma_{24}m^4(B_{13}g_{136}\mu_{13}-g_{06}\mu_{11}) + n^2\beta^2 C_p B_{113}g_{136}g_{06}\mu_{11}\mu_{13}}C_0 g_{20}g_{21}\right.$$
$$\left.\left.+\frac{2\gamma_{24}m^4(1+\mu_{13}) + 8n^2\beta^2 C_p\gamma_0^2(g_{136}-g_{06}\mu_{11})\mu_{13}}{\gamma_{24}m^4(g_{136}\mu_{13}-g_{06}\mu_{11}) - 8n^2\beta^2 C_p\gamma_0^2 g_{136}g_{06}\mu_{11}\mu_{13}}\gamma_0 g_{22}g_{24}\right]\mu_{144}\right\}\varepsilon^{-1} \tag{A.8c}$$

$$\delta_p^{(0)} = \frac{1}{\gamma_{24}}\left(\gamma_{24}^2 - \frac{\gamma_5^2}{\pi\vartheta}\varepsilon^{1/2}\right)\lambda_B - \frac{2d_2\gamma_5}{\gamma_{24}}\left(1-\frac{1}{\pi\vartheta}\varepsilon^{1/2}\right)\lambda_p - \frac{C_p\gamma_5}{2\gamma_{24}}\left(1-\frac{1}{\pi\vartheta}\varepsilon^{1/2}\right)\varepsilon^{-1} \tag{A.9a}$$

$$\delta_p^{(T)} = \frac{1}{2\gamma_{24}}[(\gamma_{24}^2\gamma_{T1} - \gamma_5\gamma_{T2}) + \frac{\gamma_5}{\pi\vartheta}(\gamma_{T2}-\gamma_5\gamma_{T1})\varepsilon^{1/2}]\Delta T \tag{A.9b}$$

$$\delta_p^{(2)} = \frac{1}{16}m^2\mu_{12}\varepsilon \tag{A.9c}$$

$$\delta_p^{(4)} = \left\{\frac{1}{16}\frac{\vartheta}{\pi}\frac{\gamma_{14}^2\gamma_{24}^2 m^8 n^4\beta^4}{g_{06}^2}g_{21}^2\varepsilon^{-3/2}\right.$$
$$\left.+\frac{m^2n^4\beta^4}{128}\left[\frac{\gamma_{24}(g_{06}\mu_{12}+8m^4\mu_{11})}{(\gamma_{24}+4n^2\beta^2 C_p B_1\mu_{20})g_{06}\mu_{11} - 4m^4\gamma_{24}B_1\mu_{20}}\right]^2\mu_{11}^2\varepsilon^3\right\} \tag{A.9d}$$

and in Eq. (A.9a) λ_B is the dimensionless axial stress of outer tube and can be written as

$$\lambda_B = \lambda_B^{(0)} - \lambda_B^{(2)}(A_{11}^{(2)}\varepsilon)^2 + \lambda_B^{(4)}(A_{11}^{(2)}\varepsilon)^4 + \cdots \tag{A.10}$$

where $(A_{11}^{(2)}\varepsilon)$ is defined by Eq. (58a), and in the above equations

$$B_{13} = \frac{m^2+9e_2n^2\beta^2}{m^2+e_2n^2\beta^2}, \quad B_{113} = \frac{9(m^2+e_2n^2\beta^2)-(m^2+9e_2n^2\beta^2)}{m^2+e_2n^2\beta^2}$$
$$g_{06} = (m^4 + 2\gamma_{212}m^2n^2\beta^2 + \gamma_{214}n^4\beta^4)$$
$$g_{08} = (\gamma_{110}m^4 + 2\gamma_{112}m^2n^2\beta^2 + \gamma_{114}n^4\beta^4) + \frac{m^2(\gamma_{120}m^2+\gamma_{122}n^2\beta^2)g_{04} + n^2\beta^2(\gamma_{131}m^2+\gamma_{133}n^2\beta^2)g_{03}}{g_{00}}$$
$$g_{00} = (\gamma_{31}+\gamma_{320}m^2+\gamma_{322}n^2\beta^2)(\gamma_{41}+\gamma_{430}m^2+\gamma_{432}n^2\beta^2) - \gamma_{331}^2m^2n^2\beta^2$$
$$g_{03} = (\gamma_{31}+\gamma_{320}m^2+\gamma_{322}n^2\beta^2)(\gamma_{41}-\gamma_{411}m^2-\gamma_{413}n^2\beta^2) - \gamma_{331}m^2(\gamma_{31}-\gamma_{310}m^2-\gamma_{312}n^2\beta^2)$$
$$g_{04} = (\gamma_{41}+\gamma_{430}m^2+\gamma_{432}n^2\beta^2)(\gamma_{31}-\gamma_{310}m^2-\gamma_{312}n^2\beta^2) - \gamma_{331}n^2\beta^2(\gamma_{41}-\gamma_{411}m^2-\gamma_{413}n^2\beta^2)$$
$$g_{136} = (m^4 + 18\gamma_{212}m^2n^2\beta^2 + 81\gamma_{214}n^4\beta^4)$$
$$g_{10} = \frac{C_0}{\gamma_0(\gamma_{114}+\gamma_{133}g_{41})16n^4\beta^4 + C_0}$$
$$g_{20} = \frac{1}{[\gamma_0(\gamma_{114}+\gamma_{133}g_{41})16n^4\beta^4+C_0][(\gamma_{114}+\gamma_{133}g_{41})16n^4\beta^4+C_0] - C_0^2}$$
$$g_{21} = \frac{[\gamma_0(\gamma_{114}+\gamma_{133}g_{41})16n^4\beta^4+C_0] + C_0\chi_1^2}{[\gamma_0(\gamma_{114}+\gamma_{133}g_{41})16n^4\beta^4+C_0][(\gamma_{114}+\gamma_{133}g_{41})16n^4\beta^4+C_0] - C_0^2}\mu_{11}$$
$$g_{22} = \frac{\chi_1^2[(\gamma_{114}+\gamma_{133}g_{41})16n^4\beta^4+C_0] + C_0}{[\gamma_0(\gamma_{114}+\gamma_{133}g_{41})16n^4\beta^4+C_0][(\gamma_{114}+\gamma_{133}g_{41})16n^4\beta^4+C_0] - C_0^2}\mu_{11}$$
$$g_{23} = \frac{[\gamma_0(\gamma_{114}+\gamma_{133}g_{41})16n^4\beta^4+C_0]}{[\gamma_0(\gamma_{114}+\gamma_{133}g_{41})16n^4\beta^4+C_0][(\gamma_{114}+\gamma_{133}g_{41})16n^4\beta^4+C_0] - C_0^2}$$

$$
\begin{aligned}
g_{24} &= \frac{[(\gamma_{114}+\gamma_{133}g_{41})16n^4\beta^4+C_0]}{[\gamma_0(\gamma_{114}+\gamma_{133}g_{41})16n^4\beta^4+C_0][(\gamma_{114}+\gamma_{133}g_{41})16n^4\beta^4+C_0]-C_0^2}\\
g_{41} &= \frac{\gamma_{41}-\gamma_{413}4n^2\beta^2}{\gamma_{41}+\gamma_{432}4n^2\beta^2}\\
\vartheta &= \varphi = \left[\frac{b}{2}\right]^{1/2}, \quad b = \left[\frac{\gamma_{320}^2}{\gamma_{320}\gamma_{110}-\gamma_{310}\gamma_{120}}\right]^{1/2}
\end{aligned}
\tag{A.11}
$$

and

$$
\begin{aligned}
&\mu_{11}=1+\mu d_{11}, \quad \mu_{12}=1+2\mu d_{11}, \quad \mu_{13}=1+\mu d_{13}, \quad \mu_{20}=1+\mu d_{20}, \quad \mu_{02}=1+\mu d_{02}\\
&\mu_{120}=1+\mu d_{11}+\mu d_{20}, \quad \mu_{102}=1+\mu d_{11}+\mu d_{02},\\
&\mu_{122}=2\mu_{11}^2+\mu_{12}\mu_{120}/\mu_{11}+\mu_{12}\mu_{20}, \quad \tilde{\mu}_{122}=2\mu_{11}^2+\mu_{12}\mu_{120}/\mu_{11}+(B_1+1)\mu_{12}\mu_{20}\\
&\mu_{123}=\mu_{11}\mu_{12}\mu_{20}, \quad \tilde{\mu}_{123}=B_1\mu_{11}\mu_{12}\mu_{20}, \quad \mu_{124}=\mu_{11}\mu_{20}+\mu_{120}, \quad \mu_{144}=\mu_{11}\mu_{02}+\mu_{102}
\end{aligned}
\tag{A.12}
$$

in which

$$
\begin{aligned}
d_{11} &= \frac{8}{\pi^2}\frac{\gamma_{C2}}{(\gamma_{C1}^2+m^2)(\gamma_{C2}^2+n^2)}\left[\gamma_{C1}+\left(m\sin\frac{m\pi}{2}-\gamma_{C1}\cos\frac{m\pi}{2}\right)\exp\left(-\frac{\pi\gamma_{C1}}{2}\right)\right][1-(-1)^n\exp(-\pi\gamma_{C2})]\\
d_{13} &= \frac{8}{\pi^2}\frac{\gamma_{C2}}{(\gamma_{C1}^2+m^2)(\gamma_{C2}^2+9n^2)}\left[\gamma_{C1}+\left(m\sin\frac{m\pi}{2}-\gamma_{C1}\cos\frac{m\pi}{2}\right)\exp\left(-\frac{\pi\gamma_{C1}}{2}\right)\right][1-(-1)^n\exp(-\pi\gamma_{C2})]\\
d_{20} &= \frac{4}{\pi^2}\frac{\gamma_{C1}}{(\gamma_{C1}^2+4m^2)\gamma_{C2}}\left[1-(-1)^n\exp\left(-\frac{\pi\gamma_{C1}}{2}\right)\right][1-\exp(-\pi\gamma_{C2})]\\
d_{02} &= \frac{4}{\pi^2}\frac{\gamma_{C2}}{\gamma_{C1}(\gamma_{C2}^2+4n^2)}\left[1-\exp\left(-\frac{\pi\gamma_{C1}}{2}\right)\right][1-\exp(-\pi\gamma_{C2})]
\end{aligned}
\tag{A.13}
$$

References

Batdorf, S.B., 1947. A simplified method of elastic-stability analysis for thin cylindrical shells. NACA TR-874.

Brenner, D.W., 1990. Empirical potential for hydrocarbons for use in simulating the chemical vapor deposition of diamond films. Physical Review B 42, 9458–9471.

Brenner, D.W., Shenderova, O.A., Harrison, J.A., Stuart, S.J., Ni, B., Sinnott, S.B., 2002. A second-generation reactive empirical bond order (REBO) potential energy expression for hydrocarbons. Journal of Physics: Condensed Matter 14, 783–802.

Chang, T., Geng, J.W., Guo, X., 2005a. Chirality- and size-dependent elastic properties of single-walled carbon nanotubes. Applied Physics Letters 87, 251929.

Chang, T., Guo, J.W., Guo, X., 2005b. Buckling of mutiwalled carbon nanotubes under axial compression and bending via a molecular mechanics model. Physical Review B 72, 064101.

Chang, T., Li, G., Guo, X., 2005c. Elastic axial buckling of carbon nanotubes via a molecular mechanics model. Carbon 43, 287–294.

Cumings, J., Zettl, A., 2000. Low-friction nanoscale linear bearing realized from multiwall carbon nanotubes. Science 289, 602–604.

Ding, F., 2005. Theoretical study of the stability of defects in single-walled carbon nanotubes as a function of their distance from the nanotube end. Physical Review B 72, 245409.

Elliott, J.A., Sandler, J.K.W., Windle, A.H., Young, R.J., Shaffer, M.S.P., 2004. Collapse of single-wall carbon nanotubes is diameter dependent. Physical Review Letters 92, 095501.

Falvo, M.R., Clary, G.J., Taylor, R.M., Chi, V., Brooks, F.P., Washburn, S., Superfine, R., 1997. Bending and buckling of carbon nanotubes under large strain. Nature 389, 582–584.

Girifalco, L.A., 1991. Interaction potential for C_{60} molecules. Journal of Physical Chemistry 95, 5370–5371.

Girifalco, L.A., Lad, R.A., 1956. Energy of cohesion, compressibility, and the potential energy functions of graphite system. Journal of Chemical Physics 25, 693–697.

Halicioglu, T., 1998. Stress calculations for carbon nanotubes. Thin Solid Films 312, 11–14.

He, X.Q., Kitipornchai, S., Liew, K.M., 2005a. Buckling analysis of multi-walled carbon nanotubes: a continuum model accounting for van der Waals interaction. Journal of the Mechanics and Physics of Solids 53, 303–326.

He, X.Q., Kitipornchai, S., Wang, C.M., Liew, K.M., 2005b. Modeling of van der Waals force for infinitesimal deformation of multi-walled carbon nanotubes treated as cylindrical shells. International Journal of Solids and Structures 42, 6032–6047.

Hoover, W.G., 1985. Canonical dynamics: equilibrium phase-space distributions. Physical Review A 31, 1695–1697.

Iijima, S., 1991. Helical microtubes of graphitic carbon. Nature 354, 56–58.

Iijima, S., Brabec, C., Maiti, A., Bernholc, J., 1996. Structural flexibility of carbon nanotubes. Journal of Chemical Physics 104, 2089–2092.

Jin, Y., Yuan, F.G., 2003. Simulation of elastic properties of single-walled carbon nanotubes. Composites Science and Technology 63, 1507–1515.

Kitipornchai, S., He, X.Q., Liew, K.M., 2005. Buckling analysis of triple-walled carbon nanotubes embedded in an elastic matrix. Journal of Applied Physics 97, 114318.

Kolmogorov, A.N., Crespi, V.H., 2000. Smoothest bearings: interlayer sliding in multiwalled carbon nanotubes. Physical Review Letters 85, 4727–4730.

Kudin, K.N., Scuseria, G.E., Yakobson, B.I., 2001. C2F, BN, and C nanoshell elasticity from *ab initio* computations. Physical Review B 64, 235406.

Liew, K.M., Wong, C.H., He, X.Q., Tan, M.J., Meguid, S.A., 2004. Nanomechanics of single and multiwalled carbon nanotubes. Physical Review B 69, 115429.

Lourie, O., Wagner, H.D., 1998. Evaluation of Young's modulus of carbon nanotubes by micro-Raman spectroscopy. Journal of Materials Research 13, 2418–2422.

Lu, J.P., 1997. Elastic properties of single and multilayered nanotubes. Journal of Physics and Chemistry of Solids 58, 1649–1652.

Ni, B., Sinnott, S.B., Mikulski, P.T., Harrison, J.A., 2002. Compression of carbon nanotubes filled with C_{60}, CH_4 or Ne: predictions from molecular dynamics simulations. Physical Review Letters 88, 205505.

Pantano, A., Parks, D.M., Boyce, M.C., 2004. Mechanics of deformation of single- and multi-wall carbon nanotubes. Journal of the Mechanics and Physics of Solids 52, 789–821.

Reddy, J.N., Liu, C.F., 1985. A higher-order shear deformation theory of laminated elastic shells. International Journal of Engineering Science 23, 319–330.

Ru, C.Q., 2000a. Effect of van der Waals forces on axial buckling of a double-walled carbon nanotube. Journal of Applied Physics 87, 7227–7231.

Ru, C.Q., 2000b. Effective bending stiffness of carbon nanotubes. Physical Review B 62, 9973–9976.

Ru, C.Q., 2000c. Elastic buckling of single-walled carbon nanotube ropes under high pressure. Physical Review B 62, 10405–10408.

Ru, C.Q., 2001a. Degraded axial buckling strain of multiwalled carbon nanotubes due to interlayer slips. Journal of Applied Physics 89, 3426–3433.

Ru, C.Q., 2001b. Axially compressed buckling of a doublewalled carbon nanotube embedded in an elastic medium. Journal of the Mechanics and Physics of Solids 49, 1265–1279.

Sears, A., Batra, R.C., 2006. Buckling of multiwalled carbon nanotubes under axial compression. Physical Review B 73, 085410.

Shen, H.-S., 2001. Postbuckling of shear deformable cross-ply laminated cylindrical shells under combined external pressure and axial compression. International Journal of Mechanical Sciences 43, 2493–2523.

Shen, H.-S., 2002. Postbuckling Behavior of Plates and Shells (in Chinese). Science and Technological Press, Shanghai, China.

Shen, H.-S., 2004. Postbuckling prediction of double-walled carbon nanotubes under hydrostatic pressure. International Journal of Solids and Structures 41, 2643–2657.

Shen, H.-S., Chen, T.-Y., 1988. A boundary layer theory for the buckling of thin cylindrical shells under external pressure. Applied Mathematics and Mechanics 9, 557–571.

Shen, H.-S., Chen, T.-Y., 1990. A boundary layer theory for the buckling of thin cylindrical shells under axial compression. In: Chien, W.Z., Fu, Z.Z. (Eds.), Advances of Applied Mathematics and Mechanics in China, Vol. 2. International Academic Publishers, Beijing, China, pp. 155–172.

Thomsen, C., Reich, S., Jantoljak, H., Loa, I., Syassen, K., Burghard, M., Duesberg, G.S., Roth, S., 1999. Raman spectroscopy on single- and multi-walled nanotubes under high pressure. Applied Physics A 69, 309–312.

Treacy, M.M.J., Ebbesen, T.W., Gibson, J.M., 1996. Exceptionally high Young's modulus observed for individual carbon nanotubes. Nature 381, 678–680.

Tu, Z.-C., Ou-Yang, Z.-C., 2002. Single-walled and multiwalled carbon nanotubes viewed as elastic tubes with the effective Young's moduli dependent on layer number. Physical Review B 65, 233407.

Wang, C.Y., Ru, C.Q., Mioduchowski, A., 2003a. Elastic buckling of multiwall carbon nanotubes under high pressure. Journal of Nanoscience and Nonatechnology 3, 199–208.

Wang, C.Y., Ru, C.Q., Mioduchowski, A., 2003b. Axially compressed buckling of pressured multiwall carbon nanotubes. International Journal of Solids and Structures 40, 3893–3911.

Wang, L., Zheng, Q., Liu, J.Z., Jinag, Q., 2005. Size dependence of the thin-shell model for carbon nanotubes. Physical Review Letters 95, 105501.

Wang, X., Yang, H.K., Yin, X.C., 2005a. Axially critical load of multiwall carbon nanotubes under thermal environment. Journal of Thermal Stresses 28, 185–196.

Wang, X., Yang, H.K., Dong, K., 2005b. Torsional buckling of multi-walled carbon nanotubes. Material Science and Engineering A 404, 314–322.

Wang, X., Yang, H.K., 2006. Bending stability of multiwalled carbon nanotubes. Physical Review B 73, 085409.

Waters, J.F., Riester, L., Jouzi, M., Guduru, P.R., Xu, J.M., 2004. Buckling instabilities in multiwalled carbon nanotubes under uniaxial compression. Applied Physics Letters 85, 1787–1789.

Waters, J.F., Guduru, P.R., Jouzi, M., Xu, J.M., Hanlon, T., Suresh, S., 2005. Shell buckling of individual multiwalled carbon nanotubes using nanoindentation. Applied Physics Letters 87, 193101.

Yakobson, B.I., Brabec, C.J., Bernholc, J., 1996. Nanomechanics of carbon tubes: instability beyond linear response. Physical Review Letters 76, 2511–2514.

Yang, H.K., Wang, X., 2006. Bending stability of multi-wall carbon nanotubes embedded in an elastic medium. Modelling and Simulation in Materials Science and Engineering 14, 99–116.

Zhang, C.-L., Shen, H.-S., 2006. Buckling and postbuckling analysis of single-walled carbon nanotubes in thermal environments via molecular dynamics simulation. Carbon, in press.

Zhou, O., 1994. Defects in carbon nanostructures. Science 263, 1744–1747.

Zhou, X., Zhou, J., Ou-Yang, Z.-C., 2000. Strain energy and Young's modulus of single-wall carbon nanotubes calculated from electronic energy-band theory. Physical Review B 62, 13692–13696.